AMERICAN SOCIETY FOR MICROBIOLOGY | Journal of Virology®

PATHOGENESIS AND IMMUNITY

CCR2 Regulates Vaccine-Induced Mucosal T-Cell Memory to Influenza A Virus

Woojong Lee,[a] Brock Kingstad-Bakke,[a] Ross M. Kedl,[b] Yoshihiro Kawaoka,[a] M. Suresh[a]

[a]Department of Pathobiological Sciences, University of Wisconsin–Madison, Madison, Wisconsin, USA
[b]Department of Immunology and Microbiology, School of Medicine, University of Colorado, Aurora, Colorado, USA

M. Suresh is the lead author.

ABSTRACT Elicitation of lung tissue-resident memory CD8 T cells (T_{RM}s) is a goal of T cell-based vaccines against respiratory viral pathogens, such as influenza A virus (IAV). C-C chemokine receptor type 2 (CCR2)-dependent monocyte trafficking plays an essential role in the establishment of CD8 T_{RM}s in lungs of IAV-infected mice. Here, we used a combination adjuvant-based subunit vaccine strategy that evokes multifaceted ($T_C1/T_C17/T_H1/T_H17$) IAV nucleoprotein-specific lung T_{RM}s to determine whether CCR2 and monocyte infiltration are essential for vaccine-induced T_{RM} development and protective immunity to IAV in lungs. Following intranasal vaccination, neutrophils, monocytes, conventional dendritic cells (DCs), and monocyte-derived dendritic cells internalized and processed vaccine antigen in lungs. We found that basic leucine zipper ATF-like transcription factor 3 (BATF3)-dependent DCs were essential for eliciting T cell responses, but CCR2 deficiency enhanced the differentiation of $CD127^{hi}$, KLRG-1^{lo}, $OX40^{+ve}$ $CD62L^{+ve}$, and mucosally imprinted $CD69^{+ve}$ $CD103^{+ve}$ effector and memory CD8 T cells in lungs and airways of vaccinated mice. Mechanistically, increased development of lung T_{RM}s induced by CCR2 deficiency was linked to dampened expression of T-bet but not altered TCF-1 levels or T cell receptor signaling in CD8 T cells. T1/T17 functional programming, parenchymal localization of CD8/CD4 effector and memory T cells, recall T cell responses, and protective immunity to a lethal IAV infection were unaffected in CCR2-deficient mice. Taken together, we identified a negative regulatory role for CCR2 and monocyte trafficking in mucosal imprinting and differentiation of vaccine-induced T_{RM}s. Mechanistic insights from this study may aid the development of T-cell-based vaccines against respiratory viral pathogens, including IAV and severe acute respiratory syndrome coronavirus 2 (SARS-CoV-2).

IMPORTANCE While antibody-based immunity to influenza A virus (IAV) is type and subtype specific, lung- and airway-resident memory T cells that recognize conserved epitopes in the internal viral proteins are known to provide heterosubtypic immunity. Hence, broadly protective IAV vaccines need to elicit robust T cell memory in the respiratory tract. We have developed a combination adjuvant-based IAV nucleoprotein vaccine that elicits strong CD4 and CD8 T cell memory in lungs and protects against H1N1 and H5N1 strains of IAV. In this study, we examined the mechanisms that control vaccine-induced protective memory T cells in the respiratory tract. We found that trafficking of monocytes into lungs might limit the development of antiviral lung-resident memory T cells following intranasal vaccination. These findings suggest that strategies that limit monocyte infiltration can potentiate vaccine-induced frontline T-cell immunity to respiratory viruses, such as IAV and SARS-CoV-2.

KEYWORDS CD8 T cells, tissue-resident memory, adjuvants, influenza vaccines, memory, mucosal adjuvants, subunit vaccines

Citation Lee W, Kingstad-Bakke B, Kedl RM, Kawaoka Y, Suresh M. 2021. CCR2 regulates vaccine-induced mucosal T-cell memory to influenza A virus. J Virol 95:e00530-21. https://doi.org/10.1128/JVI.00530-21.

Editor Stacey Schultz-Cherry, St. Jude Children's Research Hospital

Address correspondence to M. Suresh, sureshm@vetmed.wisc.edu.

Received 24 March 2021
Accepted 2 May 2021
Accepted manuscript posted online 5 May 2021
Published 12 July 2021

Upon respiratory infection, conventional dendritic cells (cDCs) endocytose and process antigens in the pulmonary environment and migrate to the draining lymph nodes (DLNs) to stimulate effector CD8 T cell responses (1–3). Naïve T cells recognize antigens in the context of antigen-presenting cells and undergo a distinct program of proliferation and differentiation into effector T cells, which traffic to lungs and clear the infection (4, 5). Upon trafficking to the lung tissues, effector T cells may encounter another round of antigenic stimulation by pulmonary antigen-presenting cells, including cDCs, monocyte-derived DCs, alveolar macrophages, monocytes, and neutrophils (6–9). In addition to antigenic restimulation, the inflammatory milieu may dictate differentiation and functional diversification of effector CD8 T cells in the lung, which in turn might regulate the quality, quantity, anatomical localization, and durability of T cell memory (10–12). Upon clearance of pathogens, phenotypically diverse memory CD4/CD8$^+$ T cells persist in the lungs. Some effector T cells within the lung differentiate into a subset of tissue-resident memory T cells (T_{RM}s) that can permanently reside within the lungs or migrate into draining lymph nodes (13); lung- and airway-resident CD8 T_{RM}s are crucial for providing broad heterosubtypic immunity against influenza (14–17). Additionally, some effector T cells differentiate into memory T cells that circulate between lymph and blood (T_{CM}) or between blood and peripheral tissues (T_{EM}) (18–20).

To protect individuals from respiratory pathogens, such as influenza A viruses (IAVs) and severe acute respiratory syndrome coronavirus 2 (SARS-CoV-2), vaccines need to engender balanced humoral and T cell-mediated immunity (21–26). While establishment of lung T_{RM}s is likely one of the major goals of designing effective T cell-based vaccines against respiratory pathogens, it has been challenging to elicit durable and effective mucosal T-cell immunity in the lungs by the use of currently available vaccine platforms (27, 28). While many of the current FDA-approved vaccines are administered by intramuscular or subcutaneous injections, there is emerging interest in designing intranasal vaccines, which can be directly delivered to the mucosal surface of the respiratory tract. Intranasally administered vaccines might be more effective than injected vaccines because intranasal vaccination can evoke virus-specific antibodies and memory CD8 T cells in the upper respiratory tract that can expeditiously clear the pathogens at the portal of entry. Hence, identifying safe and effective mucosal adjuvants is likely crucial to mitigate the global impact of currently circulating and newly emerging respiratory pathogens, such as SARS-CoV-2.

Understanding key cellular interactions that regulate the generation and persistence of memory T cell subsets is vital for designing effective vaccines. Several factors govern the development of CD8 T_{RM}s following an infection, and the roles of regulatory cytokines (e.g., interleukin 15 [IL-15] and transforming growth factor β [TGF-β]) and antigenic stimulation have been extensively investigated in recent years (10, 29–33). There is good evidence that pulmonary monocytes interact with effector CD8 T cells in the lung to drive T_{RM} differentiation following vaccinia or influenza virus infection (34, 35), but the underlying mechanisms are unknown. Further, it is unclear whether cellular and molecular factors that regulate T_{RM} formation during a viral infection play similar roles in the development of T_{RM}s following vaccination. Given the importance of T_{RM}s for protective immunity against respiratory viruses, it is important to elucidate whether monocytes play an important role in engendering T cell immunity following vaccination. Insights from such studies might aid in the rational development of adjuvants that can drive potent vaccine-induced T cell responses by engaging monocytes in the lungs.

Adjuplex (ADJ) is a carbomer-based nano-emulsion adjuvant that is known to elicit robust neutralizing antibodies to malarial and HIV envelope glycoproteins in mice and nonhuman primates (36, 37). We have previously reported that subunit protein formulated in ADJ protects against *Listeria monocytogenes*, vaccinia virus, and IAV in mice by enhancing DC cross-presentation (38–40). Additionally, we demonstrated that ADJ, in combination with Toll-like receptor 4 (TLR4) agonist glucopyranosyl lipid A (GLA), induces robust effector and T_{RM} CD8 and CD4 T cell responses to IAV nucleoprotein antigen and engenders effective T cell-dependent protection against H1N1 and H5N1 IAVs (41,

42). However, mechanisms underlying the development of vaccine-induced protective CD4/CD8 T_{RM}s in the respiratory tract remain largely unknown. In this study, in mice administered with a subunit vaccine formulated in ADJ plus GLA (ADJ+GLA), we have examined the identity and kinetics of the antigen-processing cell types in lungs and DLNs and then assessed the role of CCR2 and monocytes in orchestrating the differentiation of effector and memory CD8/CD4 T cells. Further, we examined whether programming of recall T cell responses and protective immunity are affected by CCR2 deficiency. We found that CCR2 plays key roles in promoting terminal differentiation of effector T cells and limiting CD103, OX40, and CD62L expression on effector and memory CD8 T cells. Despite altered differentiation of effector and memory T cells, programming of recall T cell responses and T cell-dependent protective immunity were unaffected in CCR2-deficient mice. These findings provide unique insights into immunological mechanisms that orchestrate memory T cell differentiation following mucosal vaccination against respiratory virus infection.

RESULTS

Dynamics of antigen-processing innate immune cells in lungs and draining lymph nodes and the role of BATF3-dependent DCs in T cell responses to i.n. vaccination with a subunit protein antigen. To reiterate, intranasal (i.n.) vaccination with a subunit protein formulated with a combination adjuvant (Adjuplex plus TLR4 agonist glucopyranosyl lipid A [ADJ+GLA]) elicited high numbers of T_{RM} CD8 T cells and provided robust protection against IAV (41). To better understand the role and identity of antigen-processing innate immune cells in eliciting a strong T_{RM} response, we vaccinated mice i.n. with DQ_{TM}-ovalbumin (DQ-OVA) protein formulated in ADJ+GLA; only upon proteolytic digestion, DQ-OVA emits green (DQ green) or red (DQ red) fluorescence (Fig. 1A) (43). At days 2, 5, and 8 after vaccination, we quantified DQ green$^+$/DQ red$^+$ innate immune cell subsets that contained processed DQ-OVA in lungs and DLNs by using the gating strategy shown in Fig. S1A in the supplemental material. Here, we found a trend where the percentages of DQ green$^+$/DQ red$^+$ cells were highest at day 2 but dwindled by day 8 after vaccination (Fig. 1B); total cell numbers of DQ green$^+$/DQ red$^+$ cells in lungs were not significantly different at days 2, 5, and 8 postvaccination (Fig. 1B). At days 2 and 5 after vaccination, neutrophils, monocytes, and monocyte-derived DCs constituted a substantive proportion of cells containing processed OVA in lungs (Fig. 1C). Upon calculation of the total numbers of DQ-OVA-containing innate immune subsets, we found that the lungs contained the highest number of DQ-OVA-bearing monocytes and neutrophils at day 2 postvaccination, and their numbers were reduced thereafter (Fig. 1D). In contrast, the number of DQ-OVA-bearing alveolar macrophages and migratory DCs were the highest at day 5 postimmunization (Fig. 1D). Notably, between days 2 and 8 after vaccination, the percentages of processed DQ-OVA-bearing CD103-positive (CD103^{+ve}) migratory DCs increased in both the lungs and DLNs. By day 8, DQ-OVA was predominantly detected in CD103^{+ve} DCs in DLNs (Fig. 1E).

Previous work has shown that development of migratory CD103^{+ve} DCs is dependent upon the basic leucine zipper ATF-like transcription factor 3 (BATF3), and T cell responses elicited by cross-presenting DCs are compromised in BATF3-deficient (BATF3$^{-/-}$) mice (44, 45). To assess whether BATF3-dependent migratory DCs are required to elicit CD8 T cell responses, we vaccinated wild-type (WT) and BATF3$^{-/-}$ mice with OVA formulated in ADJ+GLA. At day 8 after vaccination, we quantified OVA SIINFEKL epitope-specific CD8 T cells in lungs using major histocompatibility complex class I (MHC-I) tetramers (Fig. 1F). High numbers of SIINFEKL-specific CD8 T cells accumulated in lungs of WT mice, but the numbers of such cells were substantively reduced in lungs of BATF3$^{-/-}$ mice. These findings suggest that elicitation of the CD8 T cell response by ADJ+GLA requires BATF3 and likely BATF3-dependent migratory DCs.

Role of pulmonary monocytes in mucosal imprinting and differentiation of vaccine-induced effector CD8 T cells in the respiratory tract. Studies of T cell responses to IAV in CCR2-deficient (CCR2$^{-/-}$) mice have suggested that recruitment of monocytes into lungs might play a key role in development and maintenance of T_{RM}s

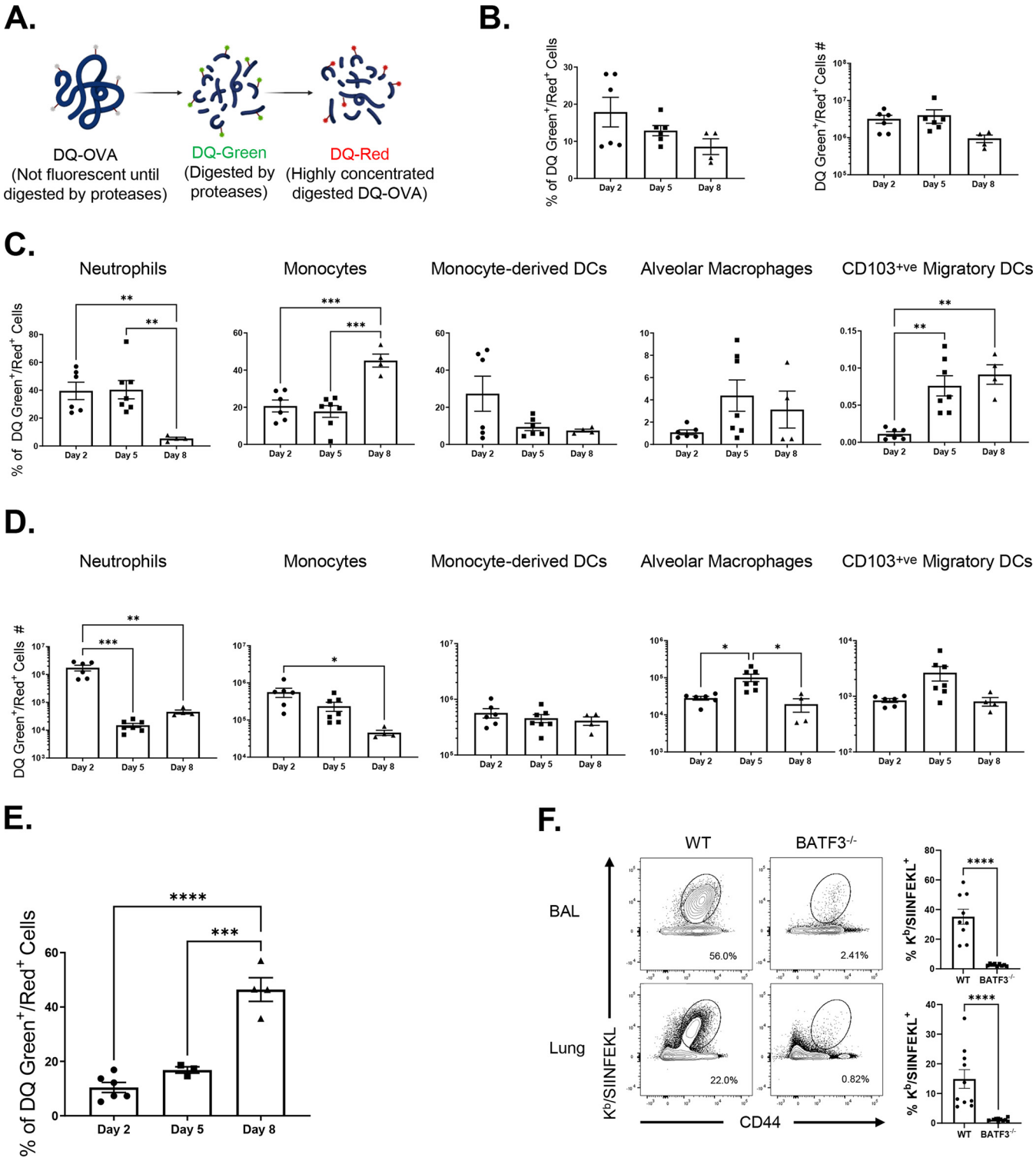

FIG 1 Dynamics of antigen processing by innate immune cells following intranasal vaccination. (A) Cartoon showing mechanism of action of DQ-OVA. Groups of C57BL/6 mice were vaccinated i.n. with DQ-OVA protein formulated in ADJ (5%) and GLA (5 μg). At days 2, 5, and 8 after immunization, single-cell suspensions of lung cells were stained with anti-CD11b, anti-Siglec-F, anti-CD11c, anti-CD64, anti-Ly6G, anti-Ly6C, anti-CD103, and anti-I-A/I-E. (B) Single-cell suspensions of lungs were analyzed for processed DQ-OVA (green and red fluorescence [DQ Green$^+$/Red$^+$]). (C) Percentages of innate immune cell subsets among all DQ Green$^+$/Red$^+$ cells. (D) Total numbers of innate immune subsets containing processed DQ-OVA in the lungs. (E) Percentages of DQ-Green$^+$ and DQ-Red$^+$ cells among CD103$^+$ migratory DCs in LNs. (F) Wild-type (WT) and BATF3-deficient (BATF3$^{-/-}$) mice were vaccinated intranasally with OVA (10 μg) formulated in ADJ (5%) plus GLA (5 μg). On day 8 after vaccination, the total number of activated OVA SIINFEKL-specific CD8 T cells in the lung and BAL fluid were quantified by staining with K^b/SIINFEKL tetramers, anti-CD8, and anti-CD44; FACS plots are gated on total live CD8 T cells, and the numbers are percentages of tetramer-binding cells among gated CD8 T cells. The data are pooled from two independent experiments (B to F). Tukey's multiple-comparison test (B to E); Mann-Whitney's U test (F). *, **, and *** indicate significance at P values of <0.05, <0.01, and <0.001, respectively.

in the respiratory tract (34, 35). Data in Fig. 1C and D show that high percentages of monocytes and monocyte-derived DCs internalized and processed protein antigen in lungs following i.n. vaccination. Therefore, it was of interest to determine whether monocytes and monocyte-derived DCs regulated CD8 T cell responses to ADJ+GLA-adjuvanted subunit vaccine. We immunized WT and CCR2$^{-/-}$ mice i.n. twice (at a 3-week interval) with influenza virus nucleoprotein (NP) formulated with ADJ+GLA. At day 8 after booster vaccination, we quantified the percentages and numbers of NP366-specific CD8 T cells in airways (bronchoalveolar lavage [BAL] fluid) and lungs. Despite the lack of monocytes in the lungs of CCR2$^{-/-}$ mice (Fig. 2A and B), the percentages and numbers of NP366-specific CD8 T cells in lungs and airways of CCR2$^{-/-}$ mice were comparable to those in WT mice (Fig. 2C and D). These data suggest that CCR2 and pulmonary monocytes are not essential for CD8 T cell responses to vaccination with ADJ+GLA.

To determine whether CCR2 deficiency altered the localization of vaccine-elicited NP366-specific CD8 T cells to the lung parenchyma, we performed intravascular staining with fluorophore-labeled CD45.2 antibodies (46); only vascular, not parenchymal, lymphocytes will demonstrate binding to anti-CD45.2. NP366-specific CD8 T cells were detected in both the lung vasculature (CD45.2^{+ve}) and lung parenchyma (CD45.2 negative [CD45.2^{-ve}]) in WT mice, but the vast majority (~96%) of NP366-specific CD8 T cells localized to the lung parenchyma (Fig. 2E). As in WT mice, the majority of NP366-specific CD8 T cells was found in lung parenchyma of vaccinated CCR2$^{-/-}$ mice (Fig. 2E), suggesting that CCR2 plays a dispensable role in regulating the vascular versus parenchymal localization of effector CD8 T cells in lungs.

We assessed whether CCR2 deficiency affected mucosal imprinting of effector CD8 T cells by examining expression of CD103 and CD69 by vaccine-induced NP366-specific CD8 T cells in lungs. While the expression of CD69 on NP366-specific CD8 T cells in airways and lungs was comparable for vaccinated WT and CCR2$^{-/-}$ mice, percentages of CD69^{+ve} CD103^{+ve} NP366-specific CD8 T cells and the median fluorescent intensities (MFI) of CD103 for CD8 T cells in CCR2$^{-/-}$ mice were significantly higher than those in lungs and airways of WT mice (Fig. 2F and G). These data suggest that monocytes might limit CD103 expression on vaccine-elicited effector CD8 T cells (Fig. 2F and G). Expression of CD103 and differentiation of T_{RM}s are regulated by antigen receptor signaling and expression of transcription factors, such as T-bet and TCF-1 (47–49). First, we quantified the levels of transcription factors T-bet and TCF-1 in NP366-specific effector CD8 T cells in lungs of vaccinated WT and CCR2$^{-/-}$ mice. The percentages of NP366-specific effector CD8 T cells that expressed elevated levels of T-bet were significantly lower in the lungs of CCR2$^{-/-}$ mice (Fig. 2H and I). Further, the expression levels of T-bet but not TCF-1 (measured by MFI) in CCR2$^{-/-}$ NP366-specific CD8 T cells were significantly lower ($P < 0.05$) than in their WT counterparts; TCF-1/T-bet ratios of MFI in CCR2$^{-/-}$ CD8 T cells in lungs were significantly higher than those in WT CD8 T cells (Fig. 2I) These data suggest that CCR2-dependent pulmonary monocyte infiltration limits mucosal imprinting of effector CD8 T cells by inducing T-bet expression.

ADJ is known to drive strong T cell receptor (TCR) signaling and terminal differentiation of effector cells, while adding GLA to ADJ dampens TCR signaling and terminal differentiation of effector cells in the respiratory tract (41). Since PD-1 expression can serve as a qualitative readout for TCR signaling in lungs of influenza-infected mice (50), we compared PD-1 expression by NP366-specific CD8 T cells in lungs of vaccinated WT and CCR2$^{-/-}$ mice. PD-1 expression by NP366-specific effector CD8 T cells in lungs and BAL fluid was comparable in WT and CCR2$^{-/-}$ mice (Fig. 3A and B). To directly determine whether CCR2 deficiency affected antigenic stimulation of CD8 T cells in DLNs and lungs, we adoptively transferred naive OVA SIINFEKL-specific TCR transgenic OT-I CD8 T cells that express enhanced green fluorescent protein (eGFP) under the control of the Nur77 promoter; eGFP expression induced by the Nur77 promoter faithfully reports ongoing TCR signaling (51). Subsequently, mice were vaccinated with OVA formulated in ADJ+GLA, and eGFP expression by donor OT-I CD8 T cells in lungs and

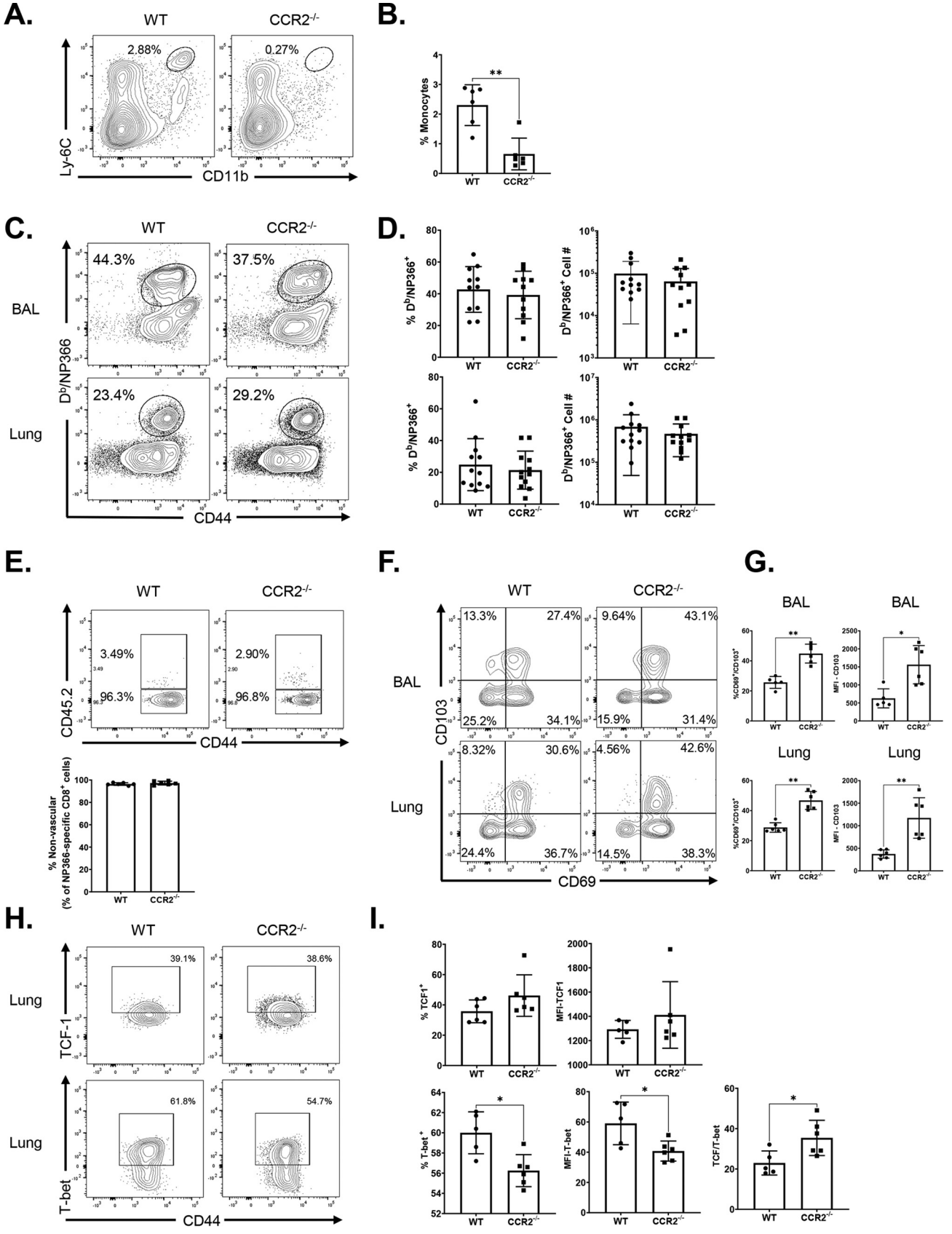

FIG 2 Effector CD8 T cell response to adjuvanted subunit vaccine in CCR2$^{-/-}$ mice. Wild-type (WT) or CCR2$^{-/-}$ mice were immunized intranasally (i.n.) twice (21 days apart) with influenza A H1N1 nucleoprotein (NP) formulated in ADJ (5%) and GLA (5 μg). To distinguish nonvascular cells from

(Continued on next page)

DLNs was quantified by flow cytometry. Here, we found that Nur77-eGFP expression by OT-I CD8 T cells in DLNs and/or lungs of WT and CCR2$^{-/-}$ mice was comparable on days 2, 5, and 8 after vaccination (Fig. 3C and D). These data suggest that CCR2 deficiency did not significantly affect antigenic stimulation of T cells in the respiratory tract. Thus, enhanced expression of CD103 in CCR2$^{-/-}$ effector CD8 T cells cannot be explained by altered TCR signaling or expression of PD-1 at least in the first 8 days after vaccination.

To determine the differentiation state of vaccine-induced NP366-specific effector CD8 T cells in the respiratory tract, we quantified CD127 and KLRG-1 expression and classified the cells as short-lived effector cells (SLECs; CD127^{lo}/KLRG-1^{hi}), memory precursor effector cells (MPECs; CD127^{hi}/KLRG-1^{lo}), transition effector cells (TEs; CD127^{hi}/KLRG1^{hi}), and early effector cells (EEs; CD127^{lo}/KLRG1^{lo}). A substantive fraction of NP366-specific CD8 T cells were MPECs in the airways and lungs of WT mice, but the relative proportions of CD127^{hi}/KLRG-1^{lo} MPECs were significantly ($P < 0.05$) higher in CCR2$^{-/-}$ mice than in WT mice, suggesting that monocytes might restrain the development of MPECs in lung (Fig. 3E and F). We further examined the differentiation status of effector CD8 T cells in CCR2$^{-/-}$ mice by measuring the expression of CD62L and OX40. In both airways and lungs, NP366-specific effector CD8 T cells in CCR2$^{-/-}$ mice exhibited significantly ($P < 0.05$) increased expression of OX40 and CD62L (Fig. 3G and H), compared to those in WT mice. Taken together, elevated expression of CD127, CD62L, and OX40 in NP366-specific CD8 T cells in CCR2$^{-/-}$ mice suggests that pulmonary monocytes might promote the differentiation of KLRG-1^{hi}/CD62L^{lo}/OX40^{lo} effector CD8 T cells in lungs.

Effect of CCR2 deficiency on vaccine-induced effector CD4 T cells in the respiratory tract. Here, we asked whether CCR2 deficiency and loss of monocytes affected the accumulation and differentiation of vaccine-induced effector CD4 T cells in the respiratory tract. At day 8 after booster vaccination with ADJ+GLA+NP, high percentages of NP311-specific CD4 T cells were detected in the airways and lungs of both WT and CCR2$^{-/-}$ mice (Fig. 4A). The percentages and total numbers of NP311-specific CD4 T cells in lungs and airways were comparable between WT and CCR2$^{-/-}$ mice. Furthermore, ~96% of effector NP311-specific CD4 T cells were found in the lung parenchyma of both WT and CCR2$^{-/-}$ mice (Fig. 4B). Unlike for effector CD8 T cells (Fig. 2), CCR2 deficiency did not affect mucosal imprinting of effector CD4 T cells in lungs; percentages of CD103^{+ve} cells among NP311-specific effector CD4 T cells were comparable in WT and CCR2$^{-/-}$ mice (Fig. 4C and D). However, CCR2 deficiency promoted the development of KLRG-1^{lo}/CD127^{hi} (MPECs) and CD62L^{+ve}/OX40^{+ve} NP311-specific effector CD4 T cells in the lungs and airways of vaccinated mice (Fig. 4E and H). Thus, CCR2 and monocytes might promote terminal differentiation of effector CD4 T cells in the lungs of vaccinated mice.

Functional polarization of vaccine-induced mucosal effector CD8 and CD4 T cells in CCR2$^{-/-}$ mice. As an index of effector differentiation, we measured granzyme B levels in NP366-specific effector CD8 T cells in the lungs of vaccinated WT and CCR2$^{-/-}$ mice at day 8 after booster vaccination. Percentages of granzyme B^{+ve} cells or the expression of granzyme B in NP366-specific CD8 T cells were not significantly different ($P < 0.05$) in lungs of vaccinated WT and CCR2$^{-/-}$ mice (Fig. 5A). We have previously reported that vaccination with ADJ+GLA+NP fostered a functionally multifac-

FIG 2 Legend (Continued)
vascular cells in the lungs, mice were injected intravenously with fluorescence-labeled anti-CD45.2 antibodies, 3 min prior to euthanasia (CD45.2^{+ve}, vascular; CD45.2^{-ve}, nonvascular.) At day 8 postvaccination, single-cell suspensions prepared from the lungs and bronchoalveolar lavage (BAL) fluid were stained with viability dye, followed by D^b/NP366 tetramers in combination with anti-CD4, anti-CD8, anti-CD44, anti-CD69, anti-CD103, anti-T-bet, and anti-TCF-1. (A and B) Lung cells were stained for innate immune cell markers as described in the legend to Fig. 1. Data are percentages of monocytes in the lungs of vaccinated WT and CCR2$^{-/-}$ mice. (C and D) FACS plots show percentages of NP366 tetramer-binding cells among CD8 T cells. (E) Percentages of vascular and nonvascular cells among NP366-specific CD8 T cells. (F to I) FACS plots are gated on D^b/NP366 tetramer-binding CD8 T cells, and numbers are percentages of CD69$^+$/CD103$^+$ (F and G) and T-bet$^+$ and TCF-1$^+$ (H and I) cells in the respective gates or quadrants. (I) MFI of TCF-1 and T-bet in NP366-specific CD8 cells in lungs and ratio of TCF-1 to T-bet MFI in NP366-specific CD8 cells in lungs. Data are pooled from three independent experiments (C and D) or represent one of three independent experiments (A, B, and F to I). Mann-Whitney U test; *, **, and *** indicate significance at *P* values of <0.05, <0.01, and <0.001, respectively.

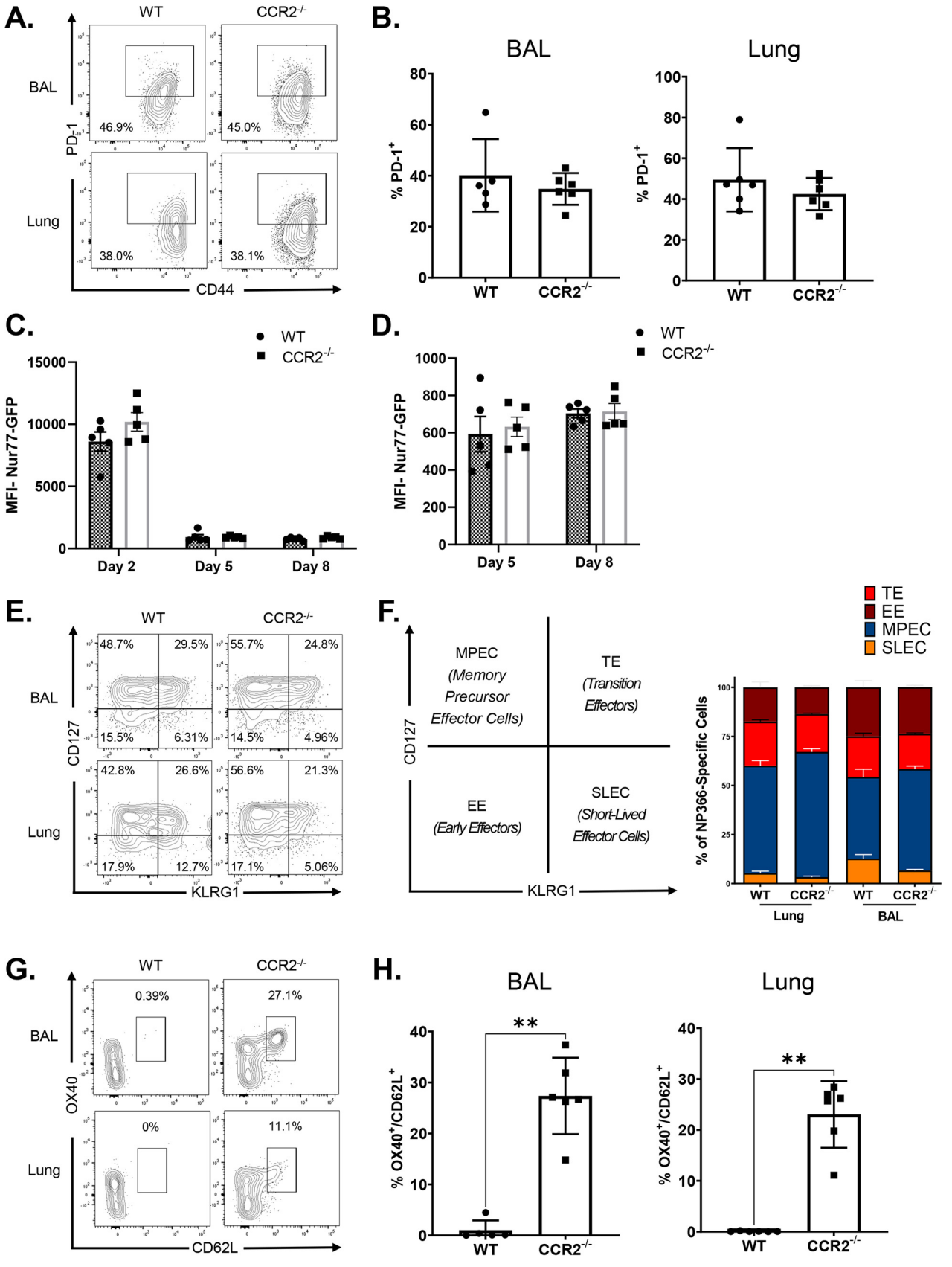

FIG 3 Role of CCR2 in regulating TCR signaling and terminal differentiation of vaccine-induced effector CD8 T cells. WT and CCR2$^{-/-}$ mice were immunized as described in the legend to Fig. 2. At day 8 postvaccination, single-cell suspensions prepared from the lungs and bronchoalveolar

(Continued on next page)

eted $T_C1/T_C17/T_{H1}/T_H17$ response in lungs (41). To investigate the role of lung monocyte recruitment in the polarization of T_C1/T_C17 effector CD8 T cells, we vaccinated cohorts of WT and CCR2$^{-/-}$ mice twice and assessed *ex vivo* cytokine production by NP366-specific CD8 T cells at day 8 after booster vaccination. Upon *ex vivo* NP366 peptide stimulation, NP366-specific effector CD8 T cells from lungs of WT and CCR2$^{-/-}$ mice produced gamma interferon (IFN-γ) and/or IL-17α (Fig. 5B). CCR2 deficiency did not affect the percentages of IFN-γ and/or IL-17α-producing CD8 T cells in lungs of vaccinated mice (Fig. 5B). Furthermore, antigen-triggered production levels of granulocyte-macrophage colony-stimulating factor (GM-CSF) by NP366-specific effector CD8 T cells in WT and CCR2$^{-/-}$ mice were similar (Fig. 5C). Likewise, CCR2 deficiency did not affect the polyfunctionality of NP366-specific effector CD8 T cells, as measured by their ability to coproduce IFN-γ, IL-2, and tumor necrosis factor alpha (TNF-α) (Fig. 5D). Similar to NP366-specific effector CD8 T cells, CCR2 deficiency did not alter the ability of NP311-specific CD4 T cells to produce IFN-γ, IL-17α, TNF-α, IL-2, or GM-CSF (Fig. 6A to C). In summary, functional polarization of $T_C1/T_C17/T_H1/T_H17$ was not affected by lack of CCR2 or monocyte recruitment into lungs of vaccinated mice.

Mucosal CD8 and CD4 T cell memory in CCR2$^{-/-}$ mice. Data in Fig. 2 and 4 demonstrate that CCR2 deficiency augmented the expression of CD103 on NP366-specific effector CD8 T cells but not NP311-specific effector CD4 T cells. Therefore, we assessed whether alteration of mucosal imprinting of effector CD8 T cells affected the development of T_{RM}s in lungs and airways. At 60 days postvaccination, the frequencies and numbers of NP366-specific memory CD8 T cells or NP311-specific memory CD4 T cells in lungs and airways of WT and CCR2$^{-/-}$ mice were largely comparable (Fig. 7A and C). Notably, the percentages of CD103^{+ve} CD69^{+ve} NP366-specific memory CD8 T cells in lungs and airways of CCR2$^{-/-}$ mice were significantly ($P < 0.05$) higher than those in WT mice (Fig. 7E). However, increased levels of CD103 on NP366-specific memory CD8 T cells in CCR2$^{-/-}$ mice minimally affected their localization in the lung parenchyma of vaccinated mice (Fig. 7B). In contrast to NP366-specific memory CD8 T cells, CCR2 deficiency affected neither CD103 expression nor parenchymal localization of NP311-specific memory CD4 T cells in lungs or airways of vaccinated mice (Fig. 7D and F). Thus, increased expression of CD103 induced by CCR2 deficiency in effector CD8 T cells was sustained in T_{RM}s in lungs and airways of vaccinated mice.

At 50 to 60 days after vaccination, we investigated whether functional polarization into T1/T17 effectors was maintained in memory T cells from CCR2$^{-/-}$ mice. Upon *ex vivo* antigenic stimulation, NP366-specific memory CD8 T cells and NP311-specific memory CD4 T cells from lungs of WT and CCR2$^{-/-}$ mice readily produced IFN-γ and/or IL-17α. The percentages of memory $T_C1/T_C17/T_H1/T_H17$ cells were comparable in WT and CCR2$^{-/-}$ mice (Fig. 7G and H). Hence, CCR2 deficiency did not affect the maintenance of T1/T17 programming in memory CD8 or CD4 T cells of vaccinated mice.

Vaccine-induced pulmonary T-cell immunity to influenza A virus in CCR2$^{-/-}$ mice. At 50 to 60 days after booster vaccination, we challenged vaccinated and unvaccinated WT and CCR2$^{-/-}$ mice with a lethal dose of the mouse-adapted PR8/H1N1 IAV and quantified recall T cell responses and viral titers in the lungs at day 6 post-virus challenge. As expected, lungs of unvaccinated WT and CCR2$^{-/-}$ mice contained high IAV titers (Fig. 8A) and mice lost 10 to 15% of body weight after viral challenge (Fig. 8B). The lungs of vaccinated WT and CCR2$^{-/-}$ mice contained up to a 6-log-lower viral burden than those in unvaccinated groups, and vaccinated mice did not exhibit de-

FIG 3 Legend (Continued)
lavage (BAL) fluid were stained with viability dye, followed by D^b/NP366 tetramers in combination with anti-CD4, anti-CD8, anti-CD44, anti-KLRG1, anti-CD127, anti-CD62L, and anti-OX40. FACS plots are gated on D^b/NP366 tetramer-binding CD8 T cells, and numbers are percentages of PD-1$^+$ (A and B), CD127$^{+/-}$/KLRG1$^{+/-}$ (E and F), and CD62L$^+$/OX40$^+$ (G and H) cells in the respective gates or quadrants. (C and D) Naïve CD45.1$^+$ Nur77-eGFP OT-I CD8 T cells were adoptively transferred into congenic CD45.2 C57BL/6 mice. Twenty-four hours after cell transfer, mice were vaccinated i.n. with OVA formulated in ADJ (5%) and GLA (5 μg). At day 2, 5, or 8 postvaccination, single-cell suspensions from mediastinal lymph nodes and lungs were stained with anti-CD8, anti-CD45.1, and K^b/SIINFEKL tetramers. The MFIs of Nur77-eGFP in donor CD45.1^{+ve} OT-I CD8 T cells were quantified by flow cytometry. The data represent one of two (C, D, G, and H) or three (A, B, E, and F) independent experiments. Mann-Whitney U test; *, **, and *** indicate significance at *P* values of <0.05, <0.01, and <0.001, respectively.

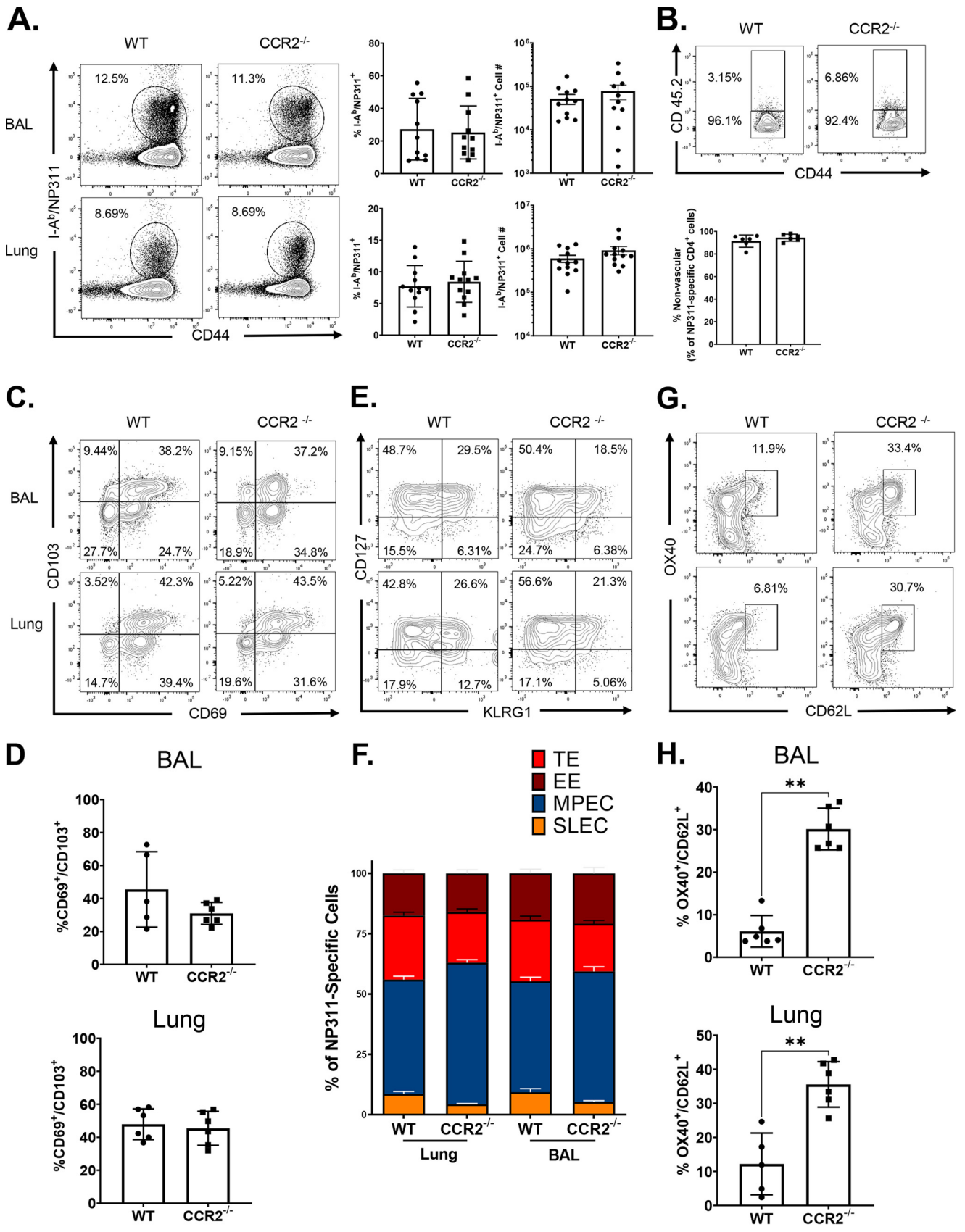

FIG 4 Effector CD4 T cell responses to adjuvanted subunit vaccine in CCR2$^{-/-}$mice. Wild-type (WT) or CCR2$^{-/-}$ mice were vaccinated as described in the legend to Fig. 2. To distinguish nonvascular cells from vascular cells in the lungs, mice were injected intravenously with fluorescence-labeled anti-CD45.2

(Continued on next page)

tectable weight loss after viral challenge (Fig. 8A and B). These data suggest that CCR2 function and monocyte recruitment are dispensable for vaccine-induced memory T cell-dependent control of IAV in mice. We then quantified recall CD8 and CD4 T cell responses in the lungs at day 6 after PR8/H1N1 challenge. The percentages and total numbers of recall NP366- and NP311-specific CD8 and CD4 T cells in lungs were comparable between WT and CCR2$^{-/-}$ groups (Fig. 8C and D). Likewise, expression of the effector molecule granzyme B was strong but comparable in NP366-specific CD8 T cells from lungs of WT and CCR2$^{-/-}$ mice (Fig. 9A). We also compared the antigen-induced cytokine-producing abilities of NP-specific recall CD8 and CD4 T cells. NP366-specific CD8 T cells and NP311-specific CD4 T cells in WT and CCR2$^{-/-}$ mice produced readily detectable but comparable levels of IL-17α, IFN-γ, TNF-α, IL-2, and GM-CSF (Fig. 9B to D and 10A to D). Taken together, data in Fig. 8 to 10 indicate that CCR2 and monocyte recruitment are dispensable for vaccine-induced T-cell-dependent protective immunity to IAV.

DISCUSSION

Lung T_{RM}s are a subset of memory T cells that reside in airways and lung parenchyma to provide the first line of antigen-specific T cell defense against respiratory pathogens (10, 11, 21). Although it is well established that conventional dendritic cells are crucial for initiating T cell priming (38, 52, 53), there are growing lines of evidence suggesting a possible role for monocytes in influencing the differentiation and persistence of T_{RM}s following recovery from respiratory viral infection (34, 35). In the current study, we have systematically documented the role of CCR2 and monocytes in orchestrating the differentiation of effector T cells, development of CD4 and CD8 T_{RM}s, and recall responses following T cell-based mucosal vaccination of mice. Data presented in this article provide new insights into the role of innate immune cells, especially pulmonary monocytes in regulating mucosal imprinting and vaccine-induced T cell immunity in the respiratory tract.

Classic inflammatory monocytes are known to limit microbial invasion by secreting cytokines, such as IL-1, IL-6, and TNF-α (54). Further, during a viral infection, under the influence of TLR agonists, inflammatory monocytes promote T_H1 responses via direct priming of naive T cells in the draining lymph nodes by cross-presentation (55–57). Importantly, antigen presentation by pulmonary monocytes to effector T cells appears to be vital for accumulation of effectors and development of T_{RM}s in lungs of virally infected mice (9, 34, 35). Further, IL-10-mediated TGF-β signaling induced by monocytes may have a critical role in the generation of T_{RM}s following vaccination (58). Studies of IAV infection show that CCR2 is required for optimal accumulation of effector CD8 T cells in lungs and development of T_{RM}s (9, 34, 35). Likewise, during a primary mucosal herpes simplex virus 2 (HSV-2) infection, activation of effector T cells in tissues was impaired in CCR2$^{-/-}$ mice (59). In the HSV-1 reactivation model, inflammatory DCs (descendants of monocytes) were required to initiate memory responses in the tissue by way of activating CD4 and CD8 T_{RM}s (60). However, we found that unlike an IAV or HSV-2 infection (9), CCR2 deficiency did not affect the magnitude of lung effector CD8 T cell responses to an adjuvanted mucosal vaccine or recall responses after viral challenge of vaccinated mice. Second, we found that CCR2 deficiency-induced loss of pulmonary monocytes led to enhancement of mucosal imprinting and development of CD103^{+ve} CD69^{+ve} CD8 effector cells and T_{RM}s in vaccinated mice. These findings suggest that mechanisms that regulate effector CD8 T cell accumulation and mucosal

FIG 4 Legend (Continued)
antibodies, 3 min prior to euthanasia (CD45.2^{+ve}, vascular; CD45.2^{-ve}, nonvascular). On day 8 after vaccination, single-cell suspensions prepared from the lungs and bronchoalveolar lavage (BAL) fluid were stained with viability dye, followed by I-A^b/NP311 tetramers in combination with anti-CD4, anti-CD8, anti-CD44, anti-CD69, anti-KLRG1, anti-CD127, anti-OX40, and anti-CD62L antibodies (A and C to H). (A) FACS plots show percentages of tetramer-binding cells among CD4 T cells. (B) Percentages of vascular and nonvascular cells among NP311-specific CD4 T cells. Data are pooled from two independent experiments (A) or represent one of three independent experiments (B to H). Mann-Whitney U test; *, **, and *** indicate significance at P values of <0.05, <0.01, and <0.001, respectively.

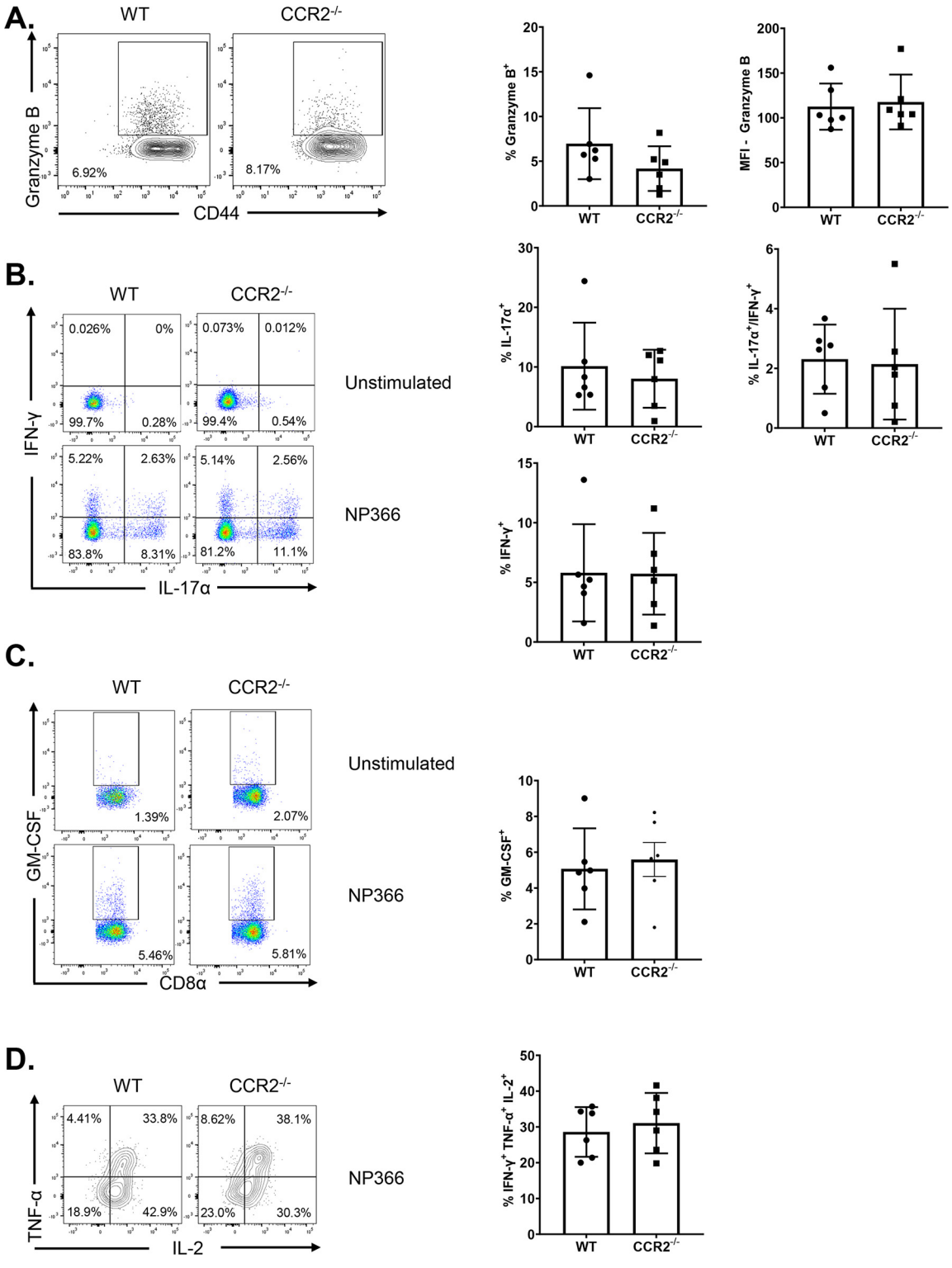

FIG 5 Functional polarization of effector CD8 T cells in vaccinated CCR2$^{-/-}$ mice. Wild-type (WT) or CCR2$^{-/-}$ mice were vaccinated as described in the legend to Fig. 2. On day 8 after vaccination, lung cells were cultured with NP366 peptide, recombinant IL-2, and brefeldin A for 5 h. The percentages of NP366-specific CD8 T cells that produced IL-17α, IFN-γ, IL-2, TNF-α, and GM-CSF were quantified by intracellular cytokine staining. (A) Percentages of IFN-γ/IL-17α-producing cells among the gated CD8 T cells. (B) Percentages of GM-CSF-producing cells among the gated CD8 T cells. (C) Percentages of IL-2/TNF-α-producing cells among the gated IFN-γ-producing CD8 T cells. Cells cultured without the NP366 peptide (unstimulated) served as a negative control. Data in each graph are mean $\pm$ standard error of the mean (SEM). Mann-Whitney U test; *, **, and *** indicate significance at *P* values of <0.05, <0.01, and <0.001 respectively. Each independent experiment had 3 to 5 mice per group. Data represent one of three independent experiments.

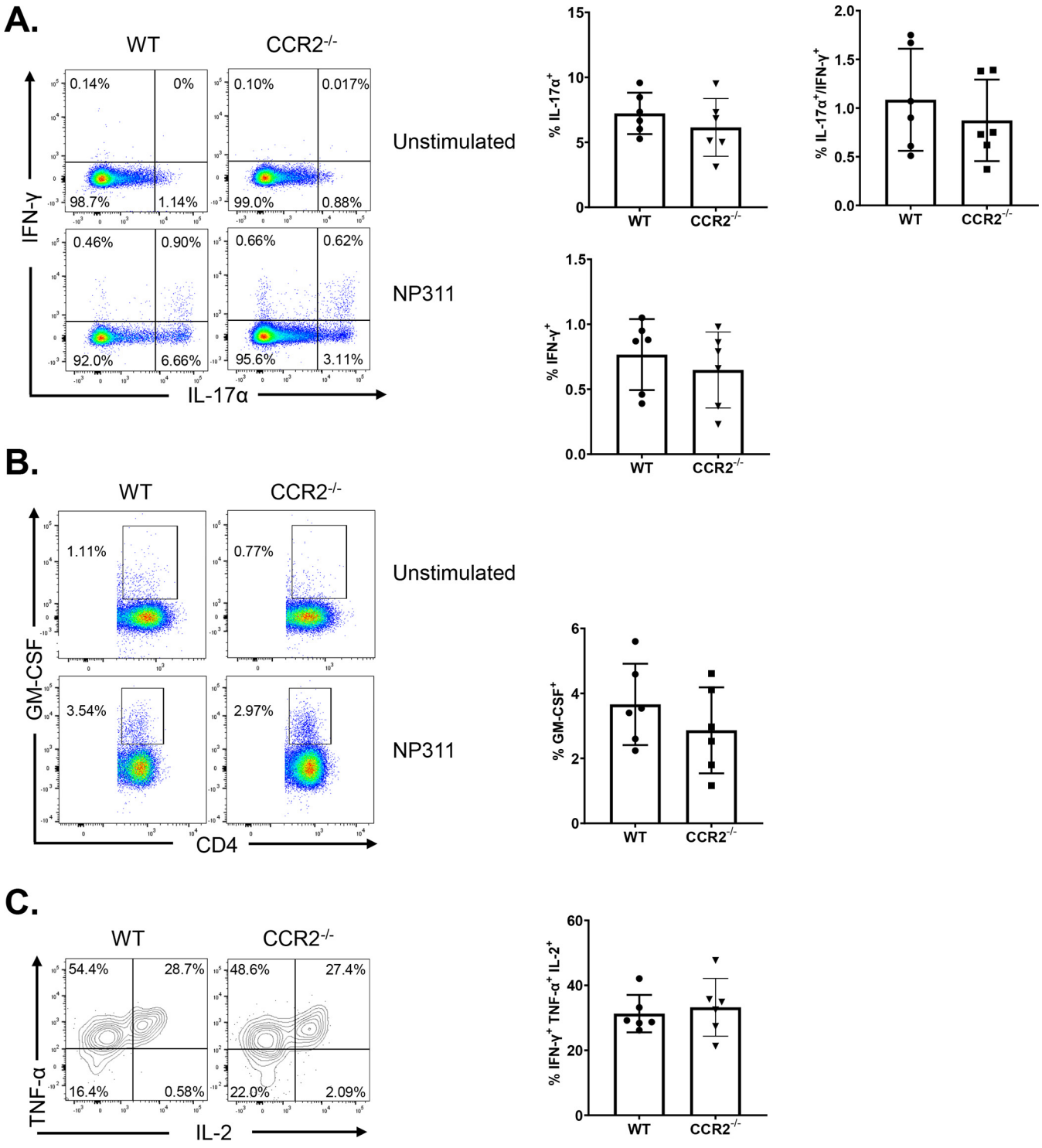

FIG 6 Functional polarization of effector CD4 T cells in vaccinated CCR2$^{-/-}$mice. Wild-type (WT) or CCR2$^{-/-}$ mice were vaccinated as described in the legend to Fig. 2. On day 8 after vaccination, lung cells were cultured with NP311 peptide, recombinant IL-2, and brefeldin A for 5 h. The percentages of NP311-specific CD4 T cells that produced IL-17α, IFN-γ, IL-2, TNF-α, and GM-CSF were quantified by intracellular cytokine staining. (A) Percentages of IFN-γ/IL-17α-producing cells among the gated CD4 T cells. (B) Percentages of GM-CSF-producing cells among the gated CD4 T cells. (C) Percentages of IL-2/TNF-α-producing cells among the gated IFN-γ-producing CD4 T cells. Cells cultured without the NP311 peptide (unstimulated) served as a negative control. Data in each graph are the mean ± SEM. Mann-Whitney U test; *, **, and *** indicate significance at *P* values of <0.05, <0.01, and <0.001, respectively. Each independent experiment had 3 to 5 mice per group. Data represent one of three independent experiments.

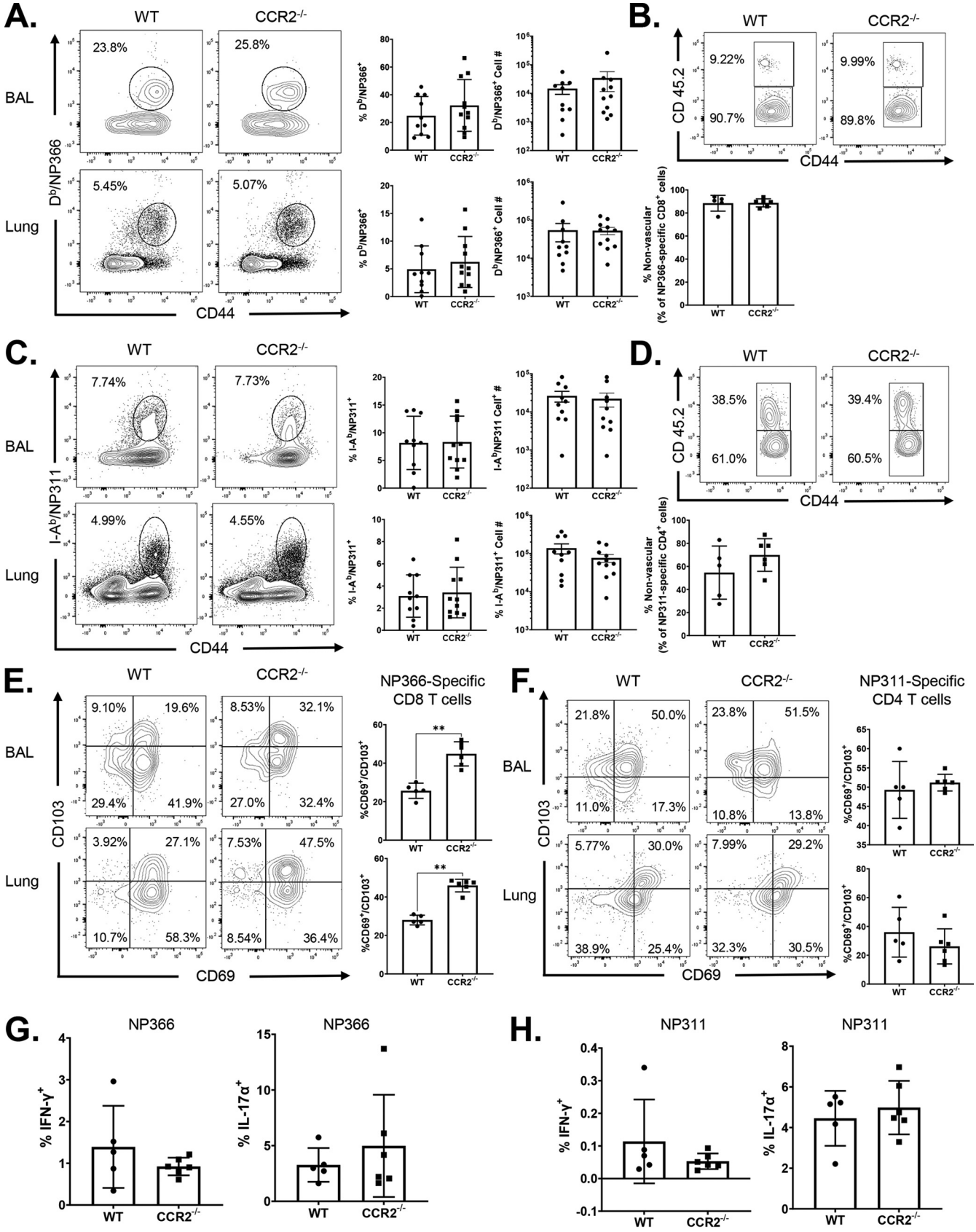

FIG 7 Vaccine-induced CD8 and CD4 T cell memory in CCR2$^{-/-}$ mice. Wild-type (WT) and CCR2$^{-/-}$ mice were vaccinated as described in the legend to Fig. 2. At 60 days after booster vaccination, the percentages and total numbers of memory NP366-specific CD8 T cells (A) and NP311-specific CD4 T cells

(Continued on next page)

imprinting are likely different in virus-infected versus vaccinated mice. Another inference is that the immunological milieus in the lungs of virus-infected and vaccinated mice are different and that the environment in vaccinated mice can promote effector expansion and T_{RM} development in the absence of monocytes. Supporting this line of argument, it is noteworthy that IAV infection triggers a dominant T1-driving inflammation but that ADJ+GLA elicits an immunological milieu that fosters T1/T17 development. It is possible that effector expansion and development of T_{RM}s in a T1 inflammatory environment but not in a T17-skewed milieu requires monocyte recruitment. Strikingly, the T1/T17-driving inflammatory milieu in lungs of ADJ+GLA-vaccinated CCR2$^{-/-}$ mice not only makes monocytes dispensable, it augments mucosal imprinting and T_{RM} development in the absence of monocytes. Factors that govern mucosal imprinting or T_{RM} development include antigen, IL-10, and TGF-β (21, 58). We found that antigenic stimulation of CD8 T cells, as monitored by measuring Nur77-eGFP expression, was not significantly different in DLNs and lungs of WT and CCR2$^{-/-}$ mice. Therefore, it is less likely that enhanced mucosal imprinting in CCR2$^{-/-}$ mice is driven by an altered magnitude of TCR signaling in lungs. From the context of the inflammatory milieu, it is noteworthy that CCR2$^{-/-}$ mice evoke a compensatory infiltration of neutrophils in the absence of monocyte recruitment (61). Because neutrophils are one of the major cell types that process vaccine antigen in lungs and can secrete an active form of TGF-β1 (62, 63), it is plausible that neutrophils can act as another major cellular source of active TGF-β1 in CCR2$^{-/-}$ mice. Follow-up studies should evaluate whether infiltration of neutrophils compensates for a lack of monocytes and provides additional TGF-β signaling in CCR2$^{-/-}$ mice, leading to augmented mucosal imprinting and development of lung T_{RM}s.

It is also noteworthy that CCR2 deficiency was associated with increased levels of less-differentiated CD127^{hi} KLRG-1^{lo} MPECs at the expense of the terminally differentiated CD127^{lo} KLRG-1^{hi} SLECs. These findings suggest that CCR2 and pulmonary monocytes promote terminal differentiation of effector T cells in lungs of vaccinated mice. CD8 T cell terminal differentiation is typically driven by antigen receptor signaling and inflammation (48). It is possible that the lack of pulmonary monocytes might have resulted in fewer antigen-presenting cells and reduced antigen encounter by T cells (9), but similar Nur77-eGFP expression in OT-I CD8 T cells and PD-1 expression on effector CD8 T cells in WT and CCR2$^{-/-}$ mice argue against this possibility. It is also plausible that loss of pulmonary monocytes in CCR2$^{-/-}$ mice results in impaired development of inflammatory monocyte-derived DCs (9), leading to a dampened inflammatory milieu in the lungs. Since T_{RM}s are believed to differentiate from CD127^{hi} cells (48), dampened inflammation and/or antigen receptor signaling in CCR2$^{-/-}$ mice might create an immunological milieu (with neutrophil-derived TGF-β) that prevents terminal differentiation but promotes development of T_{RM}s. Inflammation drives T-bet expression, and T-bet promotes terminal differentiation at the expense of T_{RM}s (48, 49, 64). Therefore, decreased expression of T-bet in CCR2$^{-/-}$ effector CD8 T cells supports the hypothesis that dampened pulmonary inflammation in the absence of monocytes/monocyte-derived DCs augments mucosal imprinting and T_{RM} development following vaccination. We have previously reported that ADJ is the vaccine component that promotes mucosal imprinting in lungs (41) and that ADJ induces a metabolically quiescent state in cross-presenting DCs (38). It will be interesting to investigate whether migratory DCs

FIG 7 Legend (Continued)
(C) were quantified in lungs and airways (BAL fluid). To distinguish nonvascular cells from vascular cells in the lungs, mice were injected intravenously with fluorescence-labeled anti-CD45.2 antibodies, 3 min prior to euthanasia (CD45.2^{+ve}, vascular; CD45.2^{-ve}, nonvascular). Single-cell suspensions from lungs or BAL fluid were stained with D^b/NP366, I-A^b/NP311, anti-CD8, anti-CD44, anti-CD103, and anti-CD69. All FACS plots in this figure are gated on tetramer-binding CD8 or CD4 T cells. (A and C) Percentages and total numbers of NP366-specific CD8 (A) and NP311-specific CD4 (C) T cells in BAL fluid and lungs. (B and D) Percentages of vascular and nonvascular cells among NP366-specific CD8 (B) and NP311-specific CD4 (D) T cells. (E and F) CD69$^+$ and/or CD103$^+$ cells among NP366-specific CD8 (E) or NP311-specific CD4 (F) T cells in lungs. (G and H) Single-cell suspensions from lungs were cultured with or without NP366 (G) or NP311 (H) peptides in the presence of recombinant IL-2 and brefeldin A for 5 h. The percentages of NP366-specific CD8 T cells or NP311-specific CD4 T cells that produced IL-17α and/or IFN-γ were quantified by intracellular cytokine staining. Data in each graph are the mean $\pm$ SEM. Mann-Whitney U test; *, **, and *** indicate significance at P values of <0.05, <0.01, and <0.001, respectively. Each independent experiment had 3 to 6 mice per group. Data are pooled from two independent experiments (A and C) or represent one of two independent experiments (B, D, and E to H).

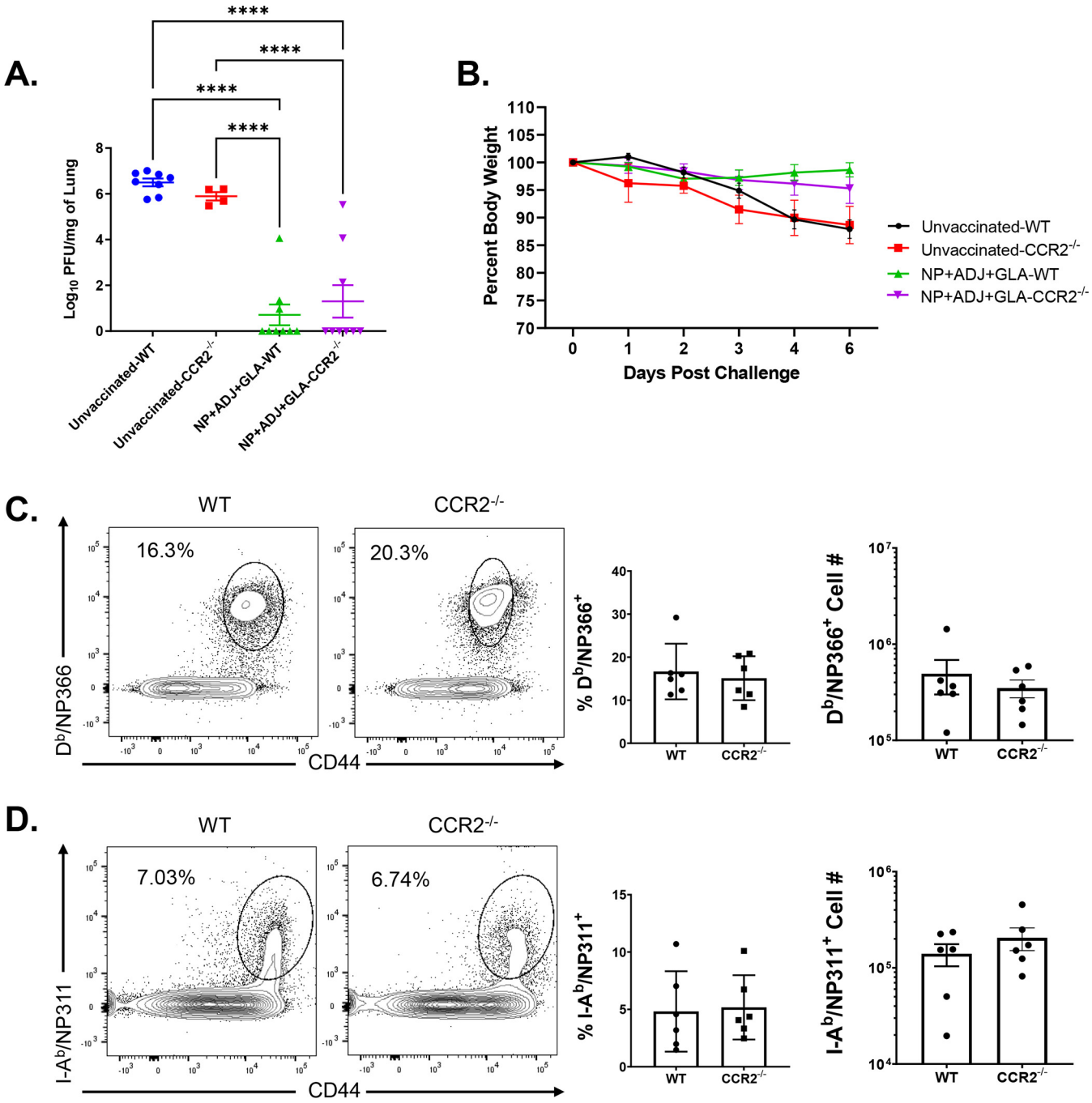

FIG 8 Vaccine-induced protective immunity to influenza A virus in wild-type (WT) and CCR2$^{-/-}$ mice. At 50 to 60 days after booster vaccination, WT or CCR2$^{-/-}$ mice were intranasally challenged with 500 PFU of the pathogenic PR8/H1N1 strain of influenza A virus. (A) Viral titers were quantified in the lungs on day 6 after challenge. (B) Following viral challenge, body weights were measured and plotted as a percentage of starting body weight prior to challenge. Single-cell suspensions prepared from lungs and bronchoalveolar lavage (BAL) fluid were stained with viability dye, followed by D^b/NP366 and I-A^b/NP311 tetramers in combination with anti-CD4, anti-CD8, and anti-CD44. (C and D) Frequencies and total numbers of NP366-specific CD8 (C) and NP311-specific CD4 (D) T cells in lungs. FACS plots are gated on total CD8 (C) or CD4 (D) T cells. Each independent experiment had 3 to 6 mice per group. Data in each graph are the mean ± SEM. The data are pooled from two independent experiments (A and B) or represent one of two independent experiments (C and D). Mann-Whitney U test; *, **, and *** indicate significance at *P* values of <0.05, <0.01, and <0.001, respectively.

in ADJ+GLA-vaccinated mice are less inflammatory and capable of augmented TGF-β-mediated preconditioning of CD8 T cells for T_{RM} fate in draining lymph nodes (65). This mechanism might make monocytes dispensable or even a limiting factor for T_{RM} development in vaccinated mice.

The most effective vaccines to date protect by inducing high levels of neutralizing

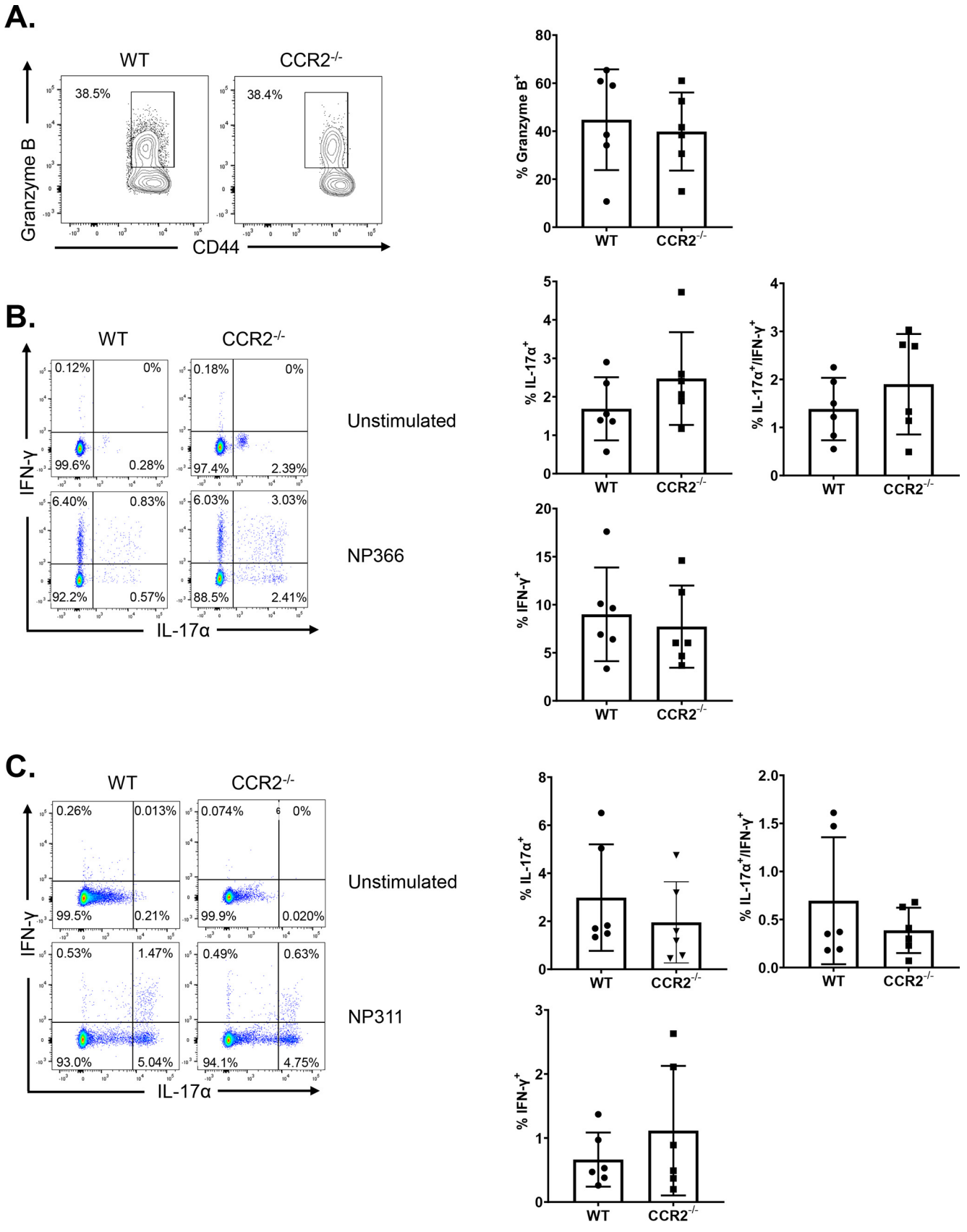

FIG 9 Effector functions of recall CD8 and CD4 T cells in influenza virus-challenged wild-type (WT) and CCR2$^{-/-}$ mice. At 50 days after booster vaccination, WT or CCR2$^{-/-}$ mice were challenged with H1N1/PR8 strain of influenza A virus. On day 6 after viral challenge, functions of antigen-specific CD4 and

(Continued on next page)

antibodies, but development of vaccines against diseases such as tuberculosis and AIDS has been a challenge for vaccinologists, because immune defense against these diseases also requires T cells. Hence, there is high interest in developing vaccine strategies that elicit robust and durable T cell immunity, especially in the mucosal tissues. We have previously reported that mucosal delivery of a subunit protein antigen formulated in a combination adjuvant (ADJ+GLA) elicited robust numbers of CD4 and CD8 T_{RM}s in lungs and airways. The current study provides two unique insights into the mechanisms that regulate development of T_{RM}s following mucosal administration of a vaccine formulated in this combination adjuvant. First, we have shown that mechanisms that regulate T_{RM} development are different for acute viral infections and vaccinations. Second, we have uncovered a negative regulatory role for pulmonary monocytes in driving mucosal imprinting and development of T_{RM}s in lungs and airways following mucosal vaccination. Results presented in this article have improved our understanding of the mechanistic underpinnings of generating effective T cell-based protective immunity in the respiratory tract. These results might pave the way for the rational development of precision adjuvants to evoke frontline T cell immunity to respiratory pathogens at the mucosal frontiers.

MATERIALS AND METHODS

Experimental animals. Seven- to 12-week-old C57BL/6J mice were purchased from restricted-access specific-pathogen-free mouse breeding colonies at the University of Wisconsin–Madison Breeding Core Facility or from Jackson Laboratory. CCR2$^{-/-}$ (stock no. 004999) and BATF3$^{-/-}$ (stock no. 013755) mice were purchased from Jackson Laboratory. B6.Nur77-GFP OT-1 mice were bred in the laboratory of Ross M. Kedl (University of Colorado, Denver).

Ethics statement. All experiments were performed in accordance with the animal protocol (protocol no. V5308 or V5564) approved by the University of Wisconsin School of Veterinary Medicine Institutional Animal Care and Use Committee. The animal committee mandates that institutions and individuals using animals for research, teaching, and/or testing must acknowledge and accept both legal and ethical responsibility for the animals under their care, as specified in the Animal Welfare Act and associated Animal Welfare Regulations and Public Health Service (PHS) policy.

Vaccination. Adjuplex (ADJ) and glucopyranosyl lipid adjuvant (GLA) were purchased from Empirion LLC (Columbus, OH) and Avanti Polar Lipids, Inc. (Alabaster, AL), respectively. All vaccinations were administered intranasally (i.n.) to anesthetized mice in 50 μl saline with 10 μg NP (influenza A H1N1 nucleoprotein [NP]; Sino Biological) or 20 μg DQ-OVA protein (Thermo Fisher Scientific) alone or with ADJ (5%) plus GLA (5 μg) (ADJ+GLA).

Adoptive transfer of Nur77-eGFP/OT-I CD8 T cells. Single-cell suspensions of spleens and lymph nodes (LNs) from Nur77-eGFP OT-I (CD45.1^{+ve}) mice containing 1×10^3 (for vaccinated mice) or 1×10^6 (for unvaccinated mice) transgenic CD8$^+$ T cells were injected intravenously into sex-matched congenic CD45.2 C57BL/6 mice. At 24 h later, mice were intranasally vaccinated with OVA formulated in ADJ+GLA. At days 2, 5, and 8 after vaccination, cells from lungs and mediastinal lymph nodes were stained with anti-CD8, anti-CD45.1, anti-CD44, and K^b/SIINFEKL tetramers. Nur77-eGFP expression by live OT-I CD8$^+$/CD45.1$^+$ cells was quantified directly *ex vivo* by acquisition on an LSR Fortessa flow cytometer (BD Biosciences).

Tissue processing and flow cytometry. Lungs and draining lymph nodes were processed by standard collagenase-based digestion, as previously described (41, 42). Briefly, lung tissue was minced and processed using a gentleMACS dissociator (Miltenyi Biotech) in 5 ml of 1% RPMI (RPMI medium with 1% fetal bovine serum [FBS]) containing 2 mg/ml collagenase B. Samples were incubated for 30 min at 37°C, rehomogenized, and resuspended in 1% RPMI. Subsequently, cells were spun down, resuspended in 10% RPMI, and counted in a hemocytometer. Single-cell suspensions (10^7/ml) prepared from various tissues were stained for viability with the dye eFluor 780 (eBiosciences, San Diego, CA) or Ghost Dye 780 (Tonbo Biosciences) and incubated with fluorochrome-labeled antibodies and MHC-I tetramers (see Table 1 for dilutions) at 4°C for 1 h. For staining with the I-A^b/NP311 tetramer (1:150 dilution), cells were incubated with tetramer at 37°C for 90 min, followed by staining with antibodies (listed in Table 1) for cell surface molecules at 4°C for 60 min. Following staining, cells were washed twice with fluorescence-activated cell sorter (FACS) buffer (2% bovine serum albumin [BSA] in phosphate-buffered saline [PBS]),

FIG 9 Legend (Continued)
CD8 T cells in lungs were analyzed. (A) Single-cell suspensions of lungs were stained directly *ex vivo* with D^b/NP366 tetramers along with anti-CD8, anti-CD44, and anti-granzyme B antibodies. FACS plots are gated on tetramer-binding CD8 T cells, and numbers are percentages of granzyme B^{+ve} cells among the gated population. (B and C) Single-cell suspensions of lungs were cultured with NP366 or NP311 peptides, and IFN-γ and/or IL-17α-producing CD8 or CD4 T cells were quantified by intracellular cytokine staining. Plots are gated on total CD8 and CD4 T cells, respectively. Numbers are percentages of IFN-γ and/or IL-17-α-producing cells among the gated population. Data are representative of two independent experiments. Mann-Whitney U test; *, **, and *** indicate significance at *P* values of <0.05, <0.01, and <0.001, respectively.

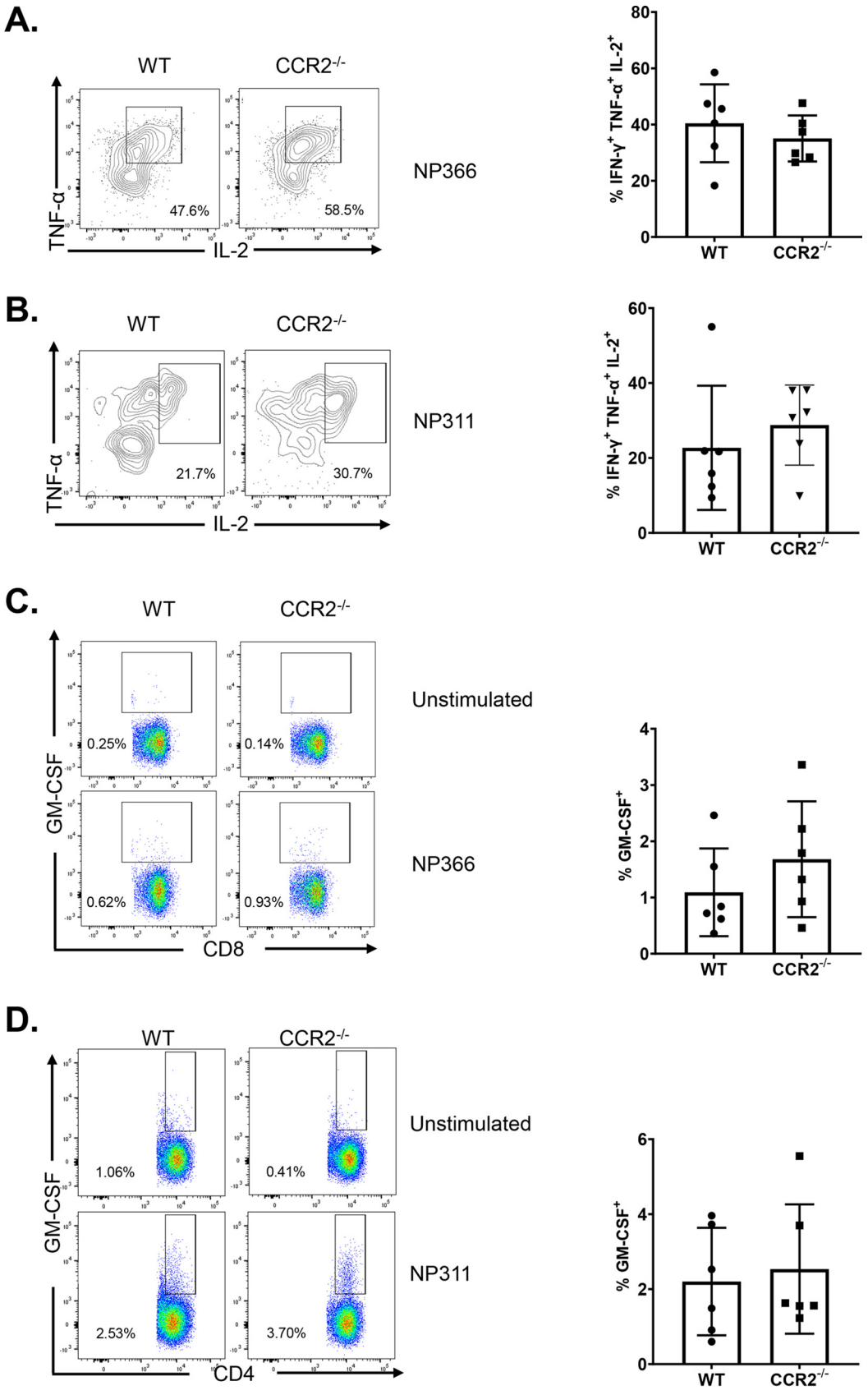

FIG 10 Polyfunctionality of recall CD8 and CD4 T cells in influenza virus-challenged wild-type (WT) and CCR2$^{-/-}$mice. At 50 to 60 days after booster vaccination, B6 or CCR2$^{-/-}$ mice were challenged with the pathogenic PR8/H1N1 strain of

(Continued on next page)

TABLE 1 List of antibodies

Antibody (dilution factor)[a]	Company	Catalog no.
Hamster anti-CD11c-BV786 conjugated (1:200)	BD Biosciences	563735
Rat anti-CD11b-BV711 conjugated (1:400)	BD Biosciences	563168
Rat anti-I-A/I-E-BV650 conjugated (1:400)	BD Biosciences	563415
Rat anti-Siglec-F-Alexa Fluor 647 conjugated (1:200)	BD Biosciences	562680
Rat anti-Ly-6G-BUV 395 conjugated (1:200)	BD Biosciences	563978
Rat anti-Ly-6C-PE-Cy7 conjugated (1:200)	BD Pharmingen	560593
Rat anti-CD8α-BUV395 conjugated (1:200)	BD Biosciences	563786
Rat anti-CD4-BUV496 conjugated (1:200)	BD Biosciences	564667
Rat anti-CD44-BV510 conjugated (1:200)	BD Biosciences	563114
Rat anti-CD62L-PE-CF594 conjugated (1:200)	BD Biosciences	562404
Hamster anti-CD69-PE-Cy7 conjugated (1:200)	BD Biosciences	553237
Hamster anti-KLRG1-BV711 conjugated (1:200)	BD Biosciences	564014
Hamster anti-CD279 (PD-1)-BV 650 conjugated (1:200)	BD Pharmingen	744546
Rat anti-IFN-γ-APC conjugated (1:400)	BD Biosciences	554413
Rat anti-TNF-α-BV421 conjugated (1:400 or 1:500)	BD Biosciences	554413
Mouse anti-granzyme B-PE conjugated (3 μl/sample)	BD Biosciences	561142
Rat anti-granzyme B-PE conjugated (3 μl/sample)	BioLegend	396406
Rat anti-CD127-BV605 conjugated (1:200)	BioLegend	135041
Hamster anti-CD103-BV605 conjugated (1:200)	BioLegend	121433
Mouse anti-CX3CR1-BV785 conjugated (1:200)	BioLegend	SA011F11
Rat anti-GM-CSF PE-Cy7 conjugated (1:200)	BioLegend	505412
Rat anti-IL-17A-FITC conjugated (1:200)	BioLegend	506908
Rat anti-CD127-PerCP/Cyanine5.5 conjugated (1:150)	BioLegend	135022
Rat anti-IL-2 PE/Dazzle 594 conjugated (1:200)	BioLegend	503840
Mouse anti-CD64 (FcγRI)-PerCP-Cy5.5 conjugated	BioLegend	139308
Rabbit TCF1-Alexa Fluor 488 conjugated (1:100)	Cell Signaling Technology	6444S
Mouse anti-CD45.2-violetFluor 450 conjugated (3 μg/mouse)	Tonbo Biosciences	75-0454-U100
Rat anti-OX40 (CD134)-PerCP-Cyanine5.5 conjugated (1:200)	Tonbo Biosciences	65-1341-U025
APC-conjugated H2-K^b tetramers bearing the ovalbumin peptide SIINFEKL	NIH Tetramer Core Facility at Emory University	
PE or BV421-conjugated I-A^b tetramers bearing the NP peptide NP311 (QVYSLIRPNENPAHK)	NIH Tetramer Core Facility at Emory University	
APC-conjugated-H-2-D^b tetramers bearing the NP peptide NP366 (ASNENMDTM)	NIH Tetramer Core Facility at Emory University	

[a]PE, phycoerythrin; APC, allophycocyanin; FITC, fluorescein isothiocyanate; PerCP, peridinin chlorophyll protein; BV, brilliant violet.

fixed with 2% paraformaldehyde for 20 min, transferred to FACS buffer, and acquired on an LSR Fortessa flow cytometer. Flow cytometry data were analyzed with FlowJo software (TreeStar, Ashland, OR).

Influenza virus challenge studies and viral titration. For viral challenge studies, vaccinated mice were intranasally challenged with 500 PFU of A/PR8/8/1934 (H1N1) strain of influenza A virus diluted in 50 μl PBS (39, 41, 42). On day 6 after influenza virus challenge, the viral loads in lungs were quantified by a plaque assay using Madin-Darby canine kidney (MDCK) cells, as previously described (41).

Intracellular staining for granzyme B and transcription factors. To stain for granzyme B or transcription factors, single-cell suspensions were first stained for viability with LiveDead eFlour 780 stain (eBioscience) or Ghost Dye red 780 (Tonbo Biosciences) for 30 min and then stained with antibodies and tetramers diluted in brilliant stain buffer (BD Biosciences) for 60 min. Samples were then fixed, permeabilized, and subsequently stained for transcription factors using a transcription factor staining kit (eBioscience) with the antibodies (listed in Table 1) diluted in Perm/Wash buffer. All samples were acquired on an LSR Fortessa flow cytometer and analyzed with FlowJo V.10 software.

Intracellular cytokine staining. For intracellular cytokine staining, one million cells were plated in flat-bottom tissue-culture-treated 96-well plates (Corning). Cells were stimulated for 5 h at 37°C in the presence of brefeldin A (1 μl/ml, GolgiPlug; BD Biosciences) and human recombinant IL-2 (10 U/well), with or without NP311 or NP366 peptides (synthesized from GenScript) at 0.2 μg/ml. After peptide stim-

FIG 10 Legend (Continued)
influenza A virus. Single-cell suspensions of lungs from challenged mice were *ex vivo* stimulated with NP366 (A and C) or NP311 peptides (B and D). The percentages of NP366-stimulated CD8 T cells that coproduced IFN-γ, TNF-α, and IL-2 (A) or GM-CSF (C) were quantified by intracellular cytokine staining. Graphs show the percentages of cytokine-producing cells among the gated CD8 T cells. IL-2- and TNF-α-coproducing cells were gated on IFN-γ-producing CD8 T cells. The percentages of NP311-stimulated CD4 T cells that coproduced IFN-γ, TNF-α, and IL-2 (B) or GM-CSF (D) were quantified by intracellular cytokine staining. Graphs show the percentages of cytokine-producing cells among the gated CD4 T cells. IL-2- and TNF-α-coproducing cells were among the gated IFN-γ-producing CD4 T cells. Data are representative of two independent experiments. Mann-Whitney U test; *, **, and *** indicate significance at *P* values of <0.05, <0.01, and <0.001, respectively.

ulation, cells were stained for viability using dye LiveDead eFlour 780 stain (eBioscience) or Ghost Dye red 780 (Tonbo Biosciences) for 30 min, stained for cell surface molecules, and fixed/permeabilizated with a Cytofix/Cytoperm kit (BD Biosciences, Franklin Lakes, NJ). Samples were stained with anticytokine antibodies (Table 1) diluted in Perm/Wash buffer for 30 min, washed with Perm/Wash buffer, and resuspended in FACS buffer before acquisition in an LSR Fortessa flow cytometer.

Statistical analyses. Statistical analyses were performed using GraphPad software 9 (La Jolla, CA). All comparisons were made using either the Mann-Whitney U test or a one-way analysis of variance (ANOVA) test with Tukey's corrected multiple comparisons, where *P* values of <0.05 (*), <0.01 (**), and <0.001 (***) were considered significantly different among groups.

SUPPLEMENTAL MATERIAL

Supplemental material is available online only.

SUPPLEMENTAL FILE 1, PDF file, 2.1 MB.

ACKNOWLEDGMENTS

We thank Autumn Larsen and Daisy Gates for expert technical assistance in performing viral titers. We also are grateful to Chandranaik B. Marinaik for assistance with vaccination. We gratefully acknowledge the Emory NIH Tetramer Core Facility for providing MHC-I and MHC-II tetramers. We thank Lisa Arendt for providing CCR2$^{-/-}$ mice to initiate this project. We express genuine appreciation for the efforts of the veterinary and animal care staff at University of Wisconsin–Madison.

This work was supported by PHS grant no. U01 AI124299 and R21 AI149793-01A1 and by a John E. Butler professorship to M. Suresh. Woojong Lee was supported by a predoctoral fellowship from the American Heart Association (18PRE34080150).

W.L., B.K.-B., and M.S. designed, performed, and analyzed the experiments and provided conceptual input for the manuscript. Y.K. and R.M.K. provided critical reagents for the study. W.L. and M.S. wrote the manuscript, which was proofread by all authors.

REFERENCES

1. Banchereau J, Steinman RM. 1998. Dendritic cells and the control of immunity. Nature 392:245–252. https://doi.org/10.1038/32588.
2. Henri S, Vremec D, Kamath A, Waithman J, Williams S, Benoist C, Burnham K, Saeland S, Handman E, Shortman K. 2001. The dendritic cell populations of mouse lymph nodes. J Immunol 167:741–748. https://doi.org/10.4049/jimmunol.167.2.741.
3. Villadangos JA, Heath WR. 2005. Life cycle, migration and antigen presenting functions of spleen and lymph node dendritic cells: limitations of the Langerhans cells paradigm. Semin Immunol 17:262–272. https://doi.org/10.1016/j.smim.2005.05.015.
4. Kim TS, Braciale TJ. 2009. Respiratory dendritic cell subsets differ in their capacity to support the induction of virus-specific cytotoxic CD8+ T cell responses. PLoS One 4:e4204. https://doi.org/10.1371/journal.pone.0004204.
5. Kohlmeier JE, Cookenham T, Miller SC, Roberts AD, Christensen JP, Thomsen AR, Woodland DL. 2009. CXCR3 directs antigen-specific effector CD4+ T cell migration to the lung during parainfluenza virus infection. J Immunol 183:4378–4384. https://doi.org/10.4049/jimmunol.0902022.
6. Laidlaw BJ, Cui W, Amezquita RA, Gray SM, Guan T, Lu Y, Kobayashi Y, Flavell RA, Kleinstein SH, Craft J, Kaech SM. 2015. Production of IL-10 by CD4(+) regulatory T cells during the resolution of infection promotes the maturation of memory CD8(+) T cells. Nat Immunol 16:871–879. https://doi.org/10.1038/ni.3224.
7. Pizzolla A, Nguyen THO, Smith JM, Brooks AG, Kedzieska K, Heath WR, Reading PC, Wakim LM. 2017. Resident memory CD8(+) T cells in the upper respiratory tract prevent pulmonary influenza virus infection. Sci Immunol 2:eaam6970. https://doi.org/10.1126/sciimmunol.aam6970.
8. McMaster SR, Wein AN, Dunbar PR, Hayward SL, Cartwright EK, Denning TL, Kohlmeier JE. 2018. Pulmonary antigen encounter regulates the establishment of tissue-resident CD8 memory T cells in the lung airways and parenchyma. Mucosal Immunol 11:1071–1078. https://doi.org/10.1038/s41385-018-0003-x.
9. Aldridge JR, Jr, Moseley CE, Boltz DA, Negovetich NJ, Reynolds C, Franks J, Brown SA, Doherty PC, Webster RG, Thomas PG. 2009. TNF/iNOS-producing dendritic cells are the necessary evil of lethal influenza virus infection. Proc Natl Acad Sci U S A 106:5306–5311. https://doi.org/10.1073/pnas.0900655106.
10. Masopust D, Soerens AG. 2019. Tissue-resident T cells and other resident leukocytes. Annu Rev Immunol 37:521–546. https://doi.org/10.1146/annurev-immunol-042617-053214.
11. Szabo PA, Miron M, Farber DL. 2019. Location, location, location: tissue resident memory T cells in mice and humans. Sci Immunol 4:eaas9673. https://doi.org/10.1126/sciimmunol.aas9673.
12. Duan S, Thomas PG. 2016. Balancing immune protection and immune pathology by CD8(+) T-cell responses to influenza infection. Front Immunol 7:25. https://doi.org/10.3389/fimmu.2016.00025.
13. Stolley JM, Johnston TS, Soerens AG, Beura LK, Rosato PC, Joag V, Wijeyesinghe SP, Langlois RA, Osum KC, Mitchell JS, Masopust D. 2020. Retrograde migration supplies resident memory T cells to lung-draining LN after influenza infection. J Exp Med 217:e20192197. https://doi.org/10.1084/jem.20192197.
14. Anderson KG, Masopust D. 2014. Editorial: Pulmonary resident memory CD8 T cells: here today, gone tomorrow. J Leukoc Biol 95:199–201. https://doi.org/10.1189/jlb.0913493.
15. Slutter B, Pewe LL, Kaech SM, Harty JT. 2013. Lung airway-surveilling CXCR3(hi) memory CD8(+) T cells are critical for protection against influenza A virus. Immunity 39:939–948. https://doi.org/10.1016/j.immuni.2013.09.013.
16. Slutter B, Van Braeckel-Budimir N, Abboud G, Varga SM, Salek-Ardakani S, Harty JT. 2017. Dynamics of influenza-induced lung-resident memory T cells underlie waning heterosubtypic immunity. Sci Immunol 2:eaag2031. . https://doi.org/10.1126/sciimmunol.aag2031.
17. Wu T, Hu Y, Lee YT, Bouchard KR, Benechet A, Khanna K, Cauley LS. 2014. Lung-resident memory CD8 T cells (TRM) are indispensable for optimal cross-protection against pulmonary virus infection. J Leukoc Biol 95:215–224. https://doi.org/10.1189/jlb.0313180.
18. Gerlach C, Moseman EA, Loughhead SM, Alvarez D, Zwijnenburg AJ, Waanders L, Garg R, de la Torre JC, von Andrian UH. 2016. The chemokine receptor CX3CR1 defines three antigen-experienced CD8 T cell subsets with distinct roles in immune surveillance and homeostasis. Immunity 45:1270–1284. https://doi.org/10.1016/j.immuni.2016.10.018.
19. Martin MD, Kim MT, Shan Q, Sompallae R, Xue HH, Harty JT, Badovinac VP. 2015. Phenotypic and functional alterations in circulating memory CD8 T

cells with time after primary infection. PLoS Pathog 11:e1005219. https://doi.org/10.1371/journal.ppat.1005219.
20. Hikono H, Kohlmeier JE, Takamura S, Wittmer ST, Roberts AD, Woodland DL. 2007. Activation phenotype, rather than central- or effector-memory phenotype, predicts the recall efficacy of memory CD8+ T cells. J Exp Med 204:1625–1636. https://doi.org/10.1084/jem.20070322.
21. Takamura S, Kohlmeier JE. 2019. Establishment and maintenance of conventional and circulation-driven lung-resident memory CD8(+) T cells following respiratory virus infections. Front Immunol 10:733. https://doi.org/10.3389/fimmu.2019.00733.
22. Sant AJ. 2019. The way forward: potentiating protective immunity to novel and pandemic influenza through engagement of memory CD4 T cells. J Infect Dis 219(Suppl):S30-S37. https://doi.org/10.1093/infdis/jiy666.
23. Gounder AP, Boon ACM. 2019. Influenza pathogenesis: the effect of host factors on severity of disease. J Immunol 202:341–350. https://doi.org/10.4049/jimmunol.1801010.
24. Sridhar S. 2016. Heterosubtypic T-cell immunity to influenza in humans: challenges for universal T-cell influenza vaccines. Front Immunol 7:195. https://doi.org/10.3389/fimmu.2016.00195.
25. Karlsson AC, Humbert M, Buggert M. 2020. The known unknowns of T cell immunity to COVID-19. Sci Immunol 5:eabe8063. https://doi.org/10.1126/sciimmunol.abe8063.
26. Koutsakos M, Illing PT, Nguyen THO, Mifsud NA, Crawford JC, Rizzetto S, Eltahla AA, Clemens EB, Sant S, Chua BY, Wong CY, Allen EK, Teng D, Dash P, Boyd DF, Grzelak L, Zeng W, Hurt AC, Barr I, Rockman S, Jackson DC, Kotsimbos TC, Cheng AC, Richards M, Westall GP, Loudovaris T, Mannering SI, Elliott M, Tangye SG, Wakim LM, Rossjohn J, Vijaykrishna D, Luciani F, Thomas PG, Gras S, Purcell AW, Kedzierska K. 2019. Human CD8(+) T cell cross-reactivity across influenza A, B and C viruses. Nat Immunol 20:613–625. https://doi.org/10.1038/s41590-019-0320-6.
27. Koff WC, Burton DR, Johnson PR, Walker BD, King CR, Nabel GJ, Ahmed R, Bhan MK, Plotkin SA. 2013. Accelerating next-generation vaccine development for global disease prevention. Science 340:1232910. https://doi.org/10.1126/science.1232910.
28. Foged C, Hansen J, Agger EM. 2012. License to kill: formulation requirements for optimal priming of CD8(+) CTL responses with particulate vaccine delivery systems. Eur J Pharm Sci 45:482–491. https://doi.org/10.1016/j.ejps.2011.08.016.
29. Sandau MM, Kohlmeier JE, Woodland DL, Jameson SC. 2010. IL-15 regulates both quantitative and qualitative features of the memory CD8 T cell pool. J Immunol 184:35–44. https://doi.org/10.4049/jimmunol.0803355.
30. Jung YW, Kim HG, Perry CJ, Kaech SM. 2016. CCR7 expression alters memory CD8 T-cell homeostasis by regulating occupancy in IL-7- and IL-15-dependent niches. Proc Natl Acad Sci U S A 113:8278–8283. https://doi.org/10.1073/pnas.1602899113.
31. Mohammed J, Beura LK, Bobr A, Astry B, Chicoine B, Kashem SW, Welty NE, Igyártó BZ, Wijeyesinghe S, Thompson EA, Matte C, Bartholin L, Kaplan A, Sheppard D, Bridges AG, Shlomchik WD, Masopust D, Kaplan DH. 2016. Stromal cells control the epithelial residence of DCs and memory T cells by regulated activation of TGF-beta. Nat Immunol 17:414–421. https://doi.org/10.1038/ni.3396.
32. Lee YT, Suarez-Ramirez JE, Wu T, Redman JM, Bouchard K, Hadley GA, Cauley LS. 2011. Environmental and antigen receptor-derived signals support sustained surveillance of the lungs by pathogen-specific cytotoxic T lymphocytes. J Virol 85:4085–4094. https://doi.org/10.1128/JVI.02493-10.
33. Zammit DJ, Turner DL, Klonowski KD, Lefrancois L, Cauley LS. 2006. Residual antigen presentation after influenza virus infection affects CD8 T cell activation and migration. Immunity 24:439–449. https://doi.org/10.1016/j.immuni.2006.01.015.
34. Desai P, Tahiliani V, Stanfield J, Abboud G, Salek-Ardakani S. 2018. Inflammatory monocytes contribute to the persistence of CXCR3(hi) CX3CR1(lo) circulating and lung-resident memory CD8(+) T cells following respiratory virus infection. Immunol Cell Biol 96:370–378. https://doi.org/10.1111/imcb.12006.
35. Dunbar PR, Cartwright EK, Wein AN, Tsukamoto T, Tiger Li ZR, Kumar N, Uddback IE, Hayward SL, Ueha S, Takamura S, Kohlmeier JE. 2020. Pulmonary monocytes interact with effector T cells in the lung tissue to drive TRM differentiation following viral infection. Mucosal Immunol 13:161–171. https://doi.org/10.1038/s41385-019-0224-7.
36. Anlar S, Capan Y, Hincal AA. 1993. Physico-chemical and bioadhesive properties of polyacrylic acid polymers. Pharmazie 48:285–287.
37. Menon V, Priya RS, Labranche C, Montefiori D, Mahalingam S, Kalyanaraman VS, Pal R. 2015. Characterization of protective immune response elicited by a trimeric envelope protein from an Indian clade C HIV-1 isolate in rhesus macaques. J Med Primatol 44:275–285. https://doi.org/10.1111/jmp.12178.
38. Lee W, Kingstad-Bakke B, Paulson B, Larsen A, Overmyer K, Marinaik CB, Dulli K, Toy R, Vogel G, Mueller KP, Tweed K, Walsh AJ, Russell J, Saha K, Reyes L, Skala MC, Sauer JD, Shayakhmetov DM, Coon J, Roy K, Suresh M. 2021. Carbomer-based adjuvant elicits CD8 T-cell immunity by inducing a distinct metabolic state in cross-presenting dendritic cells. PLoS Pathog 17:e1009168. https://doi.org/10.1371/journal.ppat.1009168.
39. Gasper DJ, Neldner B, Plisch EH, Rustom H, Carrow E, Imai H, Kawaoka Y, Suresh M. 2016. Effective respiratory CD8 T-cell immunity to influenza virus induced by intranasal carbomer-lecithin-adjuvanted non-replicating vaccines. PLoS Pathog 12:e1006064. https://doi.org/10.1371/journal.ppat.1006064.
40. Lee W, Larsen A, Kingstad-Bakke B, Marinaik CB, Suresh M. 2021. Combination adjuvants affect the magnitude of effector-like memory CD8 T cells and protection against listeriosis. Infect Immun https://doi.org/10.1128/IAI.00768-20.
41. Marinaik CB, Kingstad-Bakke B, Lee W, Hatta M, Sonsalla M, Larsen A, Neldner B, Gasper DJ, Kedl RM, Kawaoka Y, Suresh M. 2020. Programming multifaceted pulmonary T cell immunity by combination adjuvants. Cell Rep Med 1:100095. https://doi.org/10.1016/j.xcrm.2020.100095.
42. Kingstad-Bakke B, Toy R, Lee W, Pradhan P, Vogel G, Marinaik CB, Larsen A, Gates D, Luu T, Pandey B, Kawaoka Y, Roy K, Suresh M. 2020. Polymeric pathogen-like particles-based combination adjuvants elicit potent mucosal T cell immunity to influenza A virus. Front Immunol 11:559382. https://doi.org/10.3389/fimmu.2020.559382.
43. Blaauboer SM, Mansouri S, Tucker HR, Wang HL, Gabrielle VD, Jin L. 2015. The mucosal adjuvant cyclic di-GMP enhances antigen uptake and selectively activates pinocytosis-efficient cells in vivo. Elife 4 https://doi.org/10.7554/eLife.06670.
44. Kim EH, Woodruff MC, Grigoryan L, Maier B, Lee SH, Mandal P, Cortese M, Natrajan MS, Ravindran R, Ma H, Merad M, Gitlin AD, Mocarski ES, Jacob J, Pulendran B. 2020. Squalene emulsion-based vaccine adjuvants stimulate CD8 T cell, but not antibody responses, through a RIPK3-dependent pathway. Elife 9:e52687. https://doi.org/10.7554/eLife.52687.
45. Hildner K, Edelson BT, Purtha WE, Diamond M, Matsushita H, Kohyama M, Calderon B, Schraml BU, Unanue ER, Diamond MS, Schreiber RD, Murphy TL, Murphy KM. 2008. Batf3 deficiency reveals a critical role for CD8alpha+ dendritic cells in cytotoxic T cell immunity. Science 322:1097–1100. https://doi.org/10.1126/science.1164206.
46. Anderson KG, Sung H, Skon CN, Lefrancois L, Deisinger A, Vezys V, Masopust D. 2012. Cutting edge: intravascular staining redefines lung CD8 T cell responses. J Immunol 189:2702–2706. https://doi.org/10.4049/jimmunol.1201682.
47. Wu J, Madi A, Mieg A, Hotz-Wagenblatt A, Weisshaar N, Ma S, Mohr K, Schlimbach T, Hering M, Borgers H, Cui G. 2020. T cell factor 1 suppresses CD103+ lung tissue-resident memory T cell development. Cell Rep 31:107484. https://doi.org/10.1016/j.celrep.2020.03.048.
48. Jameson SC, Masopust D. 2018. Understanding subset diversity in T cell memory. Immunity 48:214–226. https://doi.org/10.1016/j.immuni.2018.02.010.
49. Mackay LK, Wynne-Jones E, Freestone D, Pellicci DG, Mielke LA, Newman DM, Braun A, Masson F, Kallies A, Belz GT, Carbone FR. 2015. T-box transcription factors combine with the cytokines TGF-beta and IL-15 to control tissue-resident memory T cell fate. Immunity 43:1101–1111. https://doi.org/10.1016/j.immuni.2015.11.008.
50. Wang Z, Wang S, Goplen NP, Li C, Cheon IS, Dai Q, Huang S, Shan J, Ma C, Ye Z, Xiang M, Limper AH, Porquera EC, Kohlmeier JE, Kaplan MH, Zhang N, Johnson AJ, Vassallo R, Sun J. 2019. PD-1(hi) CD8(+) resident memory T cells balance immunity and fibrotic sequelae. Sci Immunol 4:eaaw1217. https://doi.org/10.1126/sciimmunol.aaw1217.
51. Moran AE, Holzapfel KL, Xing Y, Cunningham NR, Maltzman JS, Punt J, Hogquist KA. 2011. T cell receptor signal strength in Treg and iNKT cell development demonstrated by a novel fluorescent reporter mouse. J Exp Med 208:1279–1289. https://doi.org/10.1084/jem.20110308.
52. Hao X, Kim TS, Braciale TJ. 2008. Differential response of respiratory dendritic cell subsets to influenza virus infection. J Virol 82:4908–4919. https://doi.org/10.1128/JVI.02367-07.
53. Jang YH, Seong BL. 2012. Principles underlying rational design of live attenuated influenza vaccines. Clin Exp Vaccine Res 1:35–49. https://doi.org/10.7774/cevr.2012.1.1.35.
54. van Leeuwen-Kerkhoff N, Lundberg K, Westers TM, Kordasti S, Bontkes HJ, de Gruijl TD, Lindstedt M, van de Loosdrecht AA. 2017. Transcriptional profiling reveals functional dichotomy between human slan(+) non-classical

monocytes and myeloid dendritic cells. J Leukoc Biol 102:1055–1068. https://doi.org/10.1189/jlb.3MA0117-037R.
55. Kastenmuller K, Wille-Reece U, Lindsay RW, Trager LR, Darrah PA, Flynn BJ, Becker MR, Udey MC, Clausen BE, Igyarto BZ, Kaplan DH, Kastenmüller W, Germain RN, Seder RA. 2011. Protective T cell immunity in mice following protein-TLR7/8 agonist-conjugate immunization requires aggregation, type I IFN, and multiple DC subsets. J Clin Invest 121:1782–1796. https://doi.org/10.1172/JCI45416.
56. Desch AN, Gibbings SL, Clambey ET, Janssen WJ, Slansky JE, Kedl RM, Henson PM, Jakubzick C. 2014. Dendritic cell subsets require cis-activation for cytotoxic CD8 T-cell induction. Nat Commun 5:4674. https://doi.org/10.1038/ncomms5674.
57. Larson SR, Atif SM, Gibbings SL, Thomas SM, Prabagar MG, Danhorn T, Leach SM, Henson PM, Jakubzick CV. 2016. Ly6C(+) monocyte efferocytosis and cross-presentation of cell-associated antigens. Cell Death Differ 23:997–1003. https://doi.org/10.1038/cdd.2016.24.
58. Thompson EA, Darrah PA, Foulds KE, Hoffer E, Caffrey-Carr A, Norenstedt S, Perbeck L, Seder RA, Kedl RM, Loré K. 2019. Monocytes acquire the ability to prime tissue-resident T cells via IL-10-mediated TGF-beta release. Cell Rep 28:1127–1135.e4. https://doi.org/10.1016/j.celrep.2019.06.087.
59. Iijima N, Mattei LM, Iwasaki A. 2011. Recruited inflammatory monocytes stimulate antiviral Th1 immunity in infected tissue. Proc Natl Acad Sci U S A 108:284–289. https://doi.org/10.1073/pnas.1005201108.
60. Wakim LM, Waithman J, van Rooijen N, Heath WR, Carbone FR. 2008. Dendritic cell-induced memory T cell activation in nonlymphoid tissues. Science 319:198–202. https://doi.org/10.1126/science.1151869.
61. Poo YS, Nakaya H, Gardner J, Larcher T, Schroder WA, Le TT, Major LD, Suhrbier A. 2014. CCR2 deficiency promotes exacerbated chronic erosive neutrophil-dominated chikungunya virus arthritis. J Virol 88:6862–6872. https://doi.org/10.1128/JVI.03364-13.
62. Chu HW, Trudeau JB, Balzar S, Wenzel SE. 2000. Peripheral blood and airway tissue expression of transforming growth factor beta by neutrophils in asthmatic subjects and normal control subjects. J Allergy Clin Immunol 106:1115–1123. https://doi.org/10.1067/mai.2000.110556.
63. Grotendorst GR, Smale G, Pencev D. 1989. Production of transforming growth factor beta by human peripheral blood monocytes and neutrophils. J Cell Physiol 140:396–402. https://doi.org/10.1002/jcp.1041400226.
64. Mueller SN, Mackay LK. 2016. Tissue-resident memory T cells: local specialists in immune defence. Nat Rev Immunol 16:79–89. https://doi.org/10.1038/nri.2015.3.
65. Mani V, Bromley SK, Äijö T, Mora-Buch R, Carrizosa E, Warner RD, Hamze M, Sen DR, Chasse AY, Lorant A, Griffith JW, Rahimi RA, McEntee CP, Jeffrey KL, Marangoni F, Travis MA, Lacy-Hulbert A, Luster AD, Mempel TR. 2019. Migratory DCs activate TGF-beta to precondition naive CD8(+) T cells for tissue-resident memory fate. Science 366:eaav5728. https://doi.org/10.1126/science.aav5728.